Supporting Information for:

# A Family of Cd(II) Coordination Polymers Constructed from 6-aminopicolinate and Bipyridil co-Linkers: Study of their Growth in Paper and Photoluminescent Sensing of $Fe^{3+}$ and $Zn^{2+}$ ions

Oier Pajuelo-Corral,[a]* Inmaculada Ortiz-Gómez, [b,c] Jose Angel García,[d] Antonio Rodríguez-Diéguez, [d] Iñigo Vitórica-Yrezabal,[e] Alfonso Salinas-Castillo,[b,c]* Jose Manuel Seco [e] and Javier Cepeda [e]*

[a] POLYMAT, University of the Basque Country (UPV/EHU), Joxe Mari Korta Center, 20018 Donostia-San Sebastián, Spain. [b] ECsens, Department of Analytical Chemistry, Faculty of Sciences, University of Granada, 18071, Granada, Spain. [c] Unit of Excellence in Chemistry Applied to Biomedicine and the Environment, Faculty of Sciences, University of Granada, 18071 Granada, Spain. [d] Departamento de Física, Facultad de Ciencia y Tecnología, Universidad del País Vasco/Euskal Herriko Unibertsitatea (UPV/EHU), 48940, Leioa, Spain. [e] Department of Inorganic Chemistry, Faculty of Sciences, University of Granada, 18071 Granada, Spain. [f] Department of Applied Chemistry, Faculty of Chemistry, University of the Basque Country UPV/EHU, 20018 Donostia-San Sebastian, Spain.

Contents:

S1. Chemical structure of H6apic and bipyridine-type linkers.

S2. Chemical characterization of compounds.

S3. FT-IR spectroscopy.

S4. Single-crystal X-ray diffraction.

S5. Powder X-ray diffraction.

S6. Structural details of compounds.

S7 Photoluminescent measurements.

S8. TD-DFT calculations.

S9. Sensing experiments.

S10. TD-DFT and DFT calculations on the interaction of $Zn^{2+}$ with compound **2**.

S11. Sensing in PADs.

S12. References.

## S1. Chemical structure of H6apic and bipyridine-type linkers

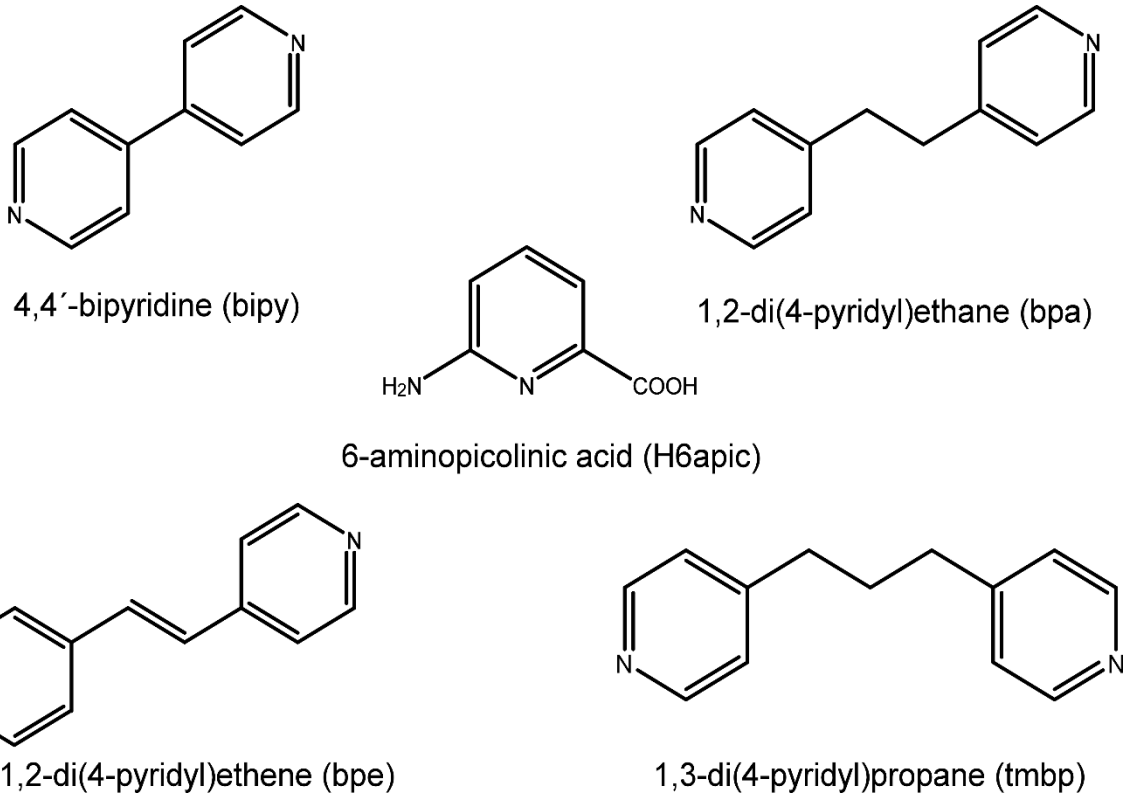


**Figure S1.** Chemical structure of the organic linkers utilized in this work for the construction of CPs.

## S2. Chemical characterization of compounds

### Thermogravimetric analysis

**Table S1.** Elemental analysis and TG/DTA curves of compound **1**.

| $[Cd(6apic)_2]_n$ | | |
|---|---|---|
| $C_{12}H_{10}CdN_4O_4$ → **M.W. = 386.64 g/mol** | | |
| **Ti–Tf** | **ΣΔm(%)** | **ΣΔm(%)$_{theor}$** |
| 370–450 | 70.5 | 70.1 (2 x 6apic) |
| 450–800 | – | – (CdO) |

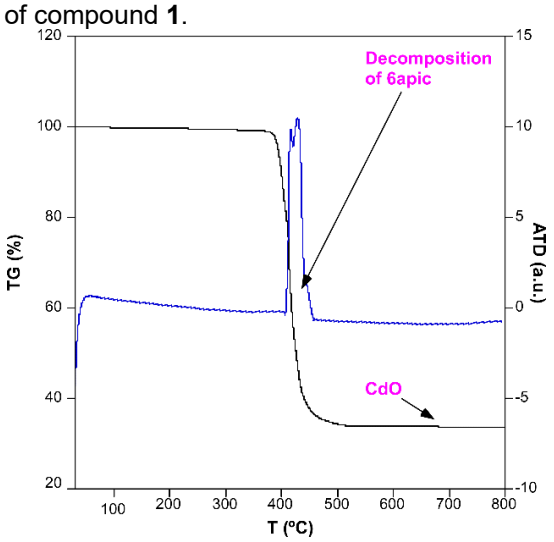


### Elemental analysis

Anal. Calc.: C, 37.28; H, 2.61; N, 14.49%. Found: C, 37.31; H, 2.68; N, 14.42%.

**Table S2.** Elemental analysis and TG/DTA curves of compound **2.**

| $\{[Cd(6apic)_2(\mu\text{-bipy})]H_2O\}_n$ | | |
|---|---|---|
| $C_{22}H_{20}CdN_6O_5$ → **M.W. = 560.85 g/mol** | | |
| **Ti–Tf** | **ΣΔm(%)** | **ΣΔm(%)$_{theor}$** |
| 150–300 | 29.6 | 31.0 ($H_2O$+bipy) |
| 350–480 | 78.6 | 79.8 (2 x 6apic) |
| 500-800 | - | -(CdO) |

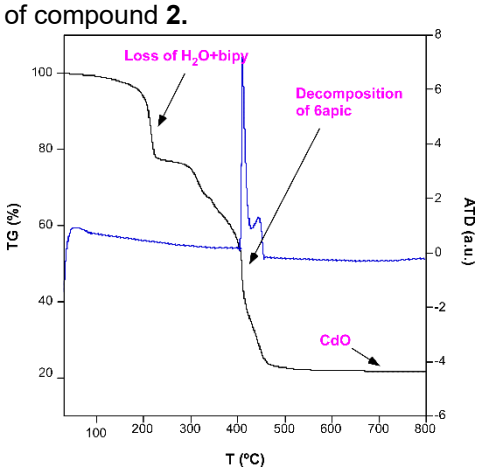


### Elemental analysis

Anal. Calc.: C, 47.11; H, 3.59; N, 14.98%. Found: C, 47.10; H, 3.50; N, 14.89%.

**Table S3.** Elemental analysis and TG/DTA curves of compound **3**.

**{[Cd(6apic)$_2$(μ-bpe)]·2 H$_2$O}$_n$**

**$C_{24}H_{24}CdN_6O_6$ → M.W. = 604.89 g/mol**

| Ti–Tf | ΣΔm(%) | ΣΔm(%)$_{theor}$ |
|---|---|---|
| 120–180 | 6.0 | 5.9 (2 x $H_2O$) |
| 220-280 | 35.2 | 35.6 (-bpe) |
| 320-450 | 80.1 | 80.2 (2 x 6apic) |
| 410–800 | – | – (CdO) |

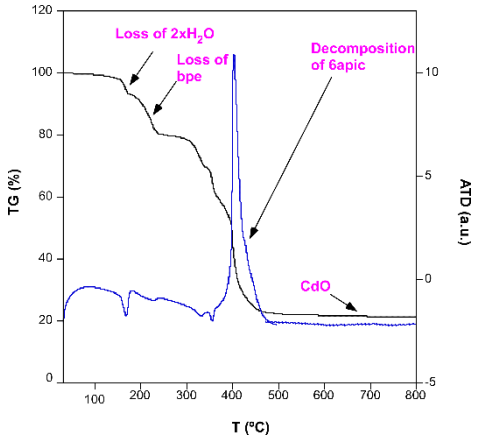


**Elemental analysis**

Anal. Calc.: C, 47.65; H, 4.00; N, 13.89%. Found: C, 47.63; H, 3.98; N, 13.92%.

**Table S4.** Elemental analysis and TG/DTA curves of compound **4**.

**[Cd(6apic)(μ-6apic)(μ-bpa)$_{0.5}$]$_n$**

**$C_{18}H_{16}CdN_5O_4$ → M.W. = 478.76 g/mol**

| Ti–Tf | ΣΔm(%) | ΣΔm(%)$_{theor}$ |
|---|---|---|
| 180-230 | 20.2 | 19.8 (0.5 bpa) |
| 300-500 | 72.6 | 72.3 (2 x 6apic) |
| 500-800 | - | CdO |

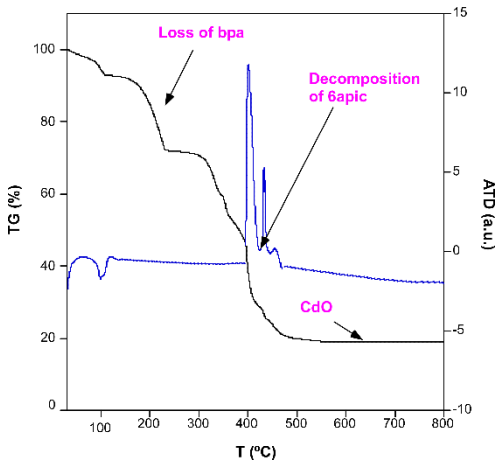


**Elemental analysis**

Anal. Calc.: C, 45.16; H, 3.37; N, 14.63%. Found: C, 45.18; H, 3.39; N, 14.60%.

**Table S5.** Elemental analysis and TG/DTA curves of compound **5**.

**$\{[Cd_2(6apic)_4(\mu\text{-}tmbp)_2]7\cdot H_2O\}_n$**

**$C_{50}H_{62}Cd_2N_{12}O_{15}$ M.W. = 1295.91 g/mol**

| Ti–Tf | ΣΔm(%) | $\Sigma\Delta m(\%)_{theor}$ |
|---|---|---|
| 80–120 | 9.2 | 9.7 (3.5 x $H_2O$) |
| 220-280 | 28.8 | 30.2 (tmbp) |
| 320-450 | 78.6 | 76.4 (2 x 6apic) |
| 410–800 | – | – (CdO) |

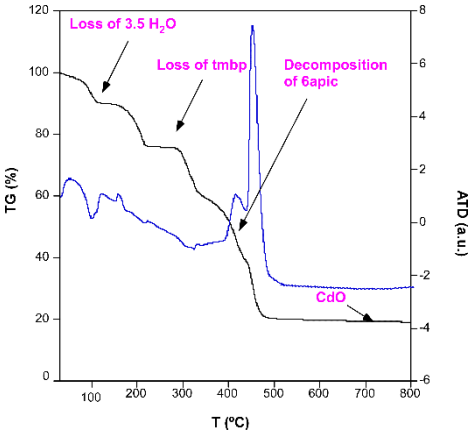


**Elemental analysis**

Anal. Calc.: C, 46.34; H, 4.82; N, 12.97%. Found: C, 46.38; H, 4.80; N, 12.95%.

## S3 FT-IR spectroscopy

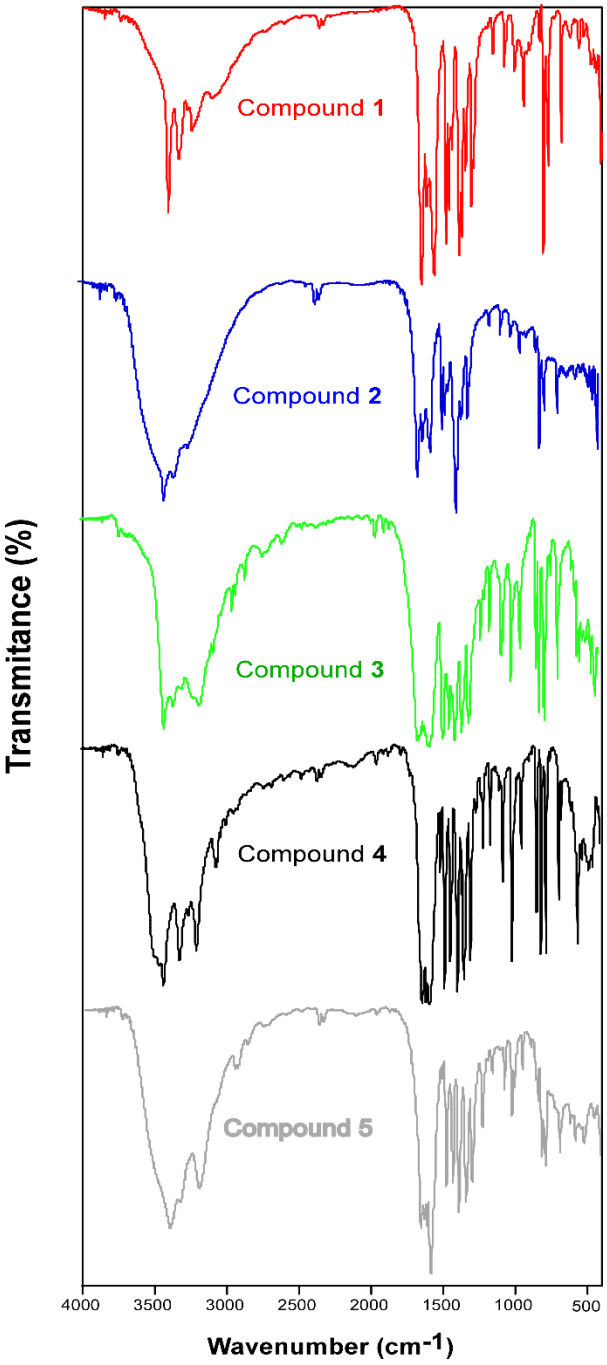


**Figure S2.** IR spectra of compounds **1**, **2**, **3**, **4**, and **5**.

## S4. Single-crystal X-ray diffraction

**Table S6.** Crystallographic data for compounds **1, 2** and **3.**

| | **1** | **2** | **3** |
|---|---|---|---|
| Empirical formula | $C_{12}H_{10}CdN_4O_4$ | $C_{22}H_{20}CdN_6O_5$ | $C_{24}H_{24}CdN_6O_6$ |
| Formula weight | 386.64 | 560.85 | 604.89 |
| Crystal system | Triclinic | Monoclinic | Monoclinic |
| Space group | $P\bar{1}$ | $P2_1/c$ | $P2_1/c$ |
| *a* (Å) | 7.9686(6) | 15.4668(2) | 9.1683(12) |
| *b* (Å) | 7.9686(6) | 16.9471(2) | 16.3792(18) |
| *c* (Å) | 19.9322(18) | 8.2657(1) | 8.5948(12) |
| *α*/ ° | 98.012(7) | 90 | 90 |
| *β*/ ° | 99.021(7) | 94.949(1) | 105.423(15) |
| *γ*/ ° | 93.425(6) | 90 | 90 |
| V (Å$^3$) | 1236.11(18) | 2158.51(5) | 1244.2(3) |
| Z | 4 | 4 | 4 |
| Reflections collected | 8333 | 17381 | 18941 |
| Unique data/parameters | 5624/380 | 4359/310 | 3707/172 |
| Rint | 0.0736 | 0.0468 | 0.0315 |
| GoF (S)[a] | 1.905 | 1.060 | 1.069 |
| $R_1$[b]/$wR^2$[c] [I>2σ(I)] | 0.1038/0.3152 | 0.0340/0.0969 | 0.0323/0.0810 |
| $R_1$[b]/$wR^2$[c] [all] | 0.1072/0.3184 | 0.0380/0.1024 | 0.0371/0.0843 |

[a] $S = [\sum w(F_0^2 - F_c^2)^2 / (N_{obs} - N_{param})]^{1/2}$. [b] $R_1 = \sum||F_0|-|F_c|| / \sum|F_0|$; [c] $wR^2 = [\sum w(F_0^2 - F_c^2)^2 / \sum wF_0^2]^{1/2}$; $w = 1/[\sigma^2(F_0^2) + (aP)^2 + bP]$ where $P = (\max(F_0^2,0) + 2Fc^2)/3$ with a = 0.0200 (**1**), 0.0640 (**2**), 0.0508 (**3**) and b = 0.3936 (**2**) and 0.4643 (**3**).

**Table S7.** Crystallographic data for compounds **4** and **5.**

| | **4** | **5** |
|---|---|---|
| Empirical formula | $C_{18}H_{16}CdN_5O_4$ | $C_{50}H_{62}Cd_2N_{12}O_{15}$ |
| Formula weight | 478.76 | 1295.91 |
| Crystal system | Monoclinic | Monoclinic |
| Space group | *I2/c* | $P2_1/c$ |
| *a* (Å) | 14.7069(2) | 21.0218(8) |
| *b* (Å) | 16.6281(2) | 12.7604(3) |
| *c* (Å) | 15.3169(2) | 23.0865(15) |
| *α*/ ° | 90 | 90 |
| *β*/ ° | 97.091(1) | 115.335(6) |
| *γ*/ ° | 90 | 90 |
| V (Å$^3$) | 3717.06(8) | 5597.2(5) |
| Z | 8 | 4 |
| Reflections collected | 12802 | 39568 |
| Unique data/parameters | 3475/263 | 11233/712 |
| Rint | 0.0275 | 0.1042 |
| GoF (S)[a] | 1.037 | 1.037 |
| $R_1$[b]/$wR^2$[c] [I>2σ(I)] | 0.0211/0.0463 | 0.0625/0.1119 |
| $R_1$[b]/$wR^2$[c] [all] | 0.0244/0.0480 | 0.1127/0.1340 |

[a] $S = [\sum w(F_0^2 - F_c^2)^2 / (N_{obs} - N_{param})]^{1/2}$. [b] $R_1 = \sum||F_0|-|F_c|| / \sum|F_0|$; [c] $wR^2 = [\sum w(F_0^2 - F_c^2)^2 / \sum wF_0^2]^{1/2}$; $w = 1/[\sigma^2(F_0^2) + (aP)^2 + bP]$ where $P = (\max(F_0^2,0) + 2Fc^2)/3$ with a = 0.0185 (**4**), 0.0396 (**5**) and b = 4.4531 (**4**).

## S5. Powder X-ray diffraction

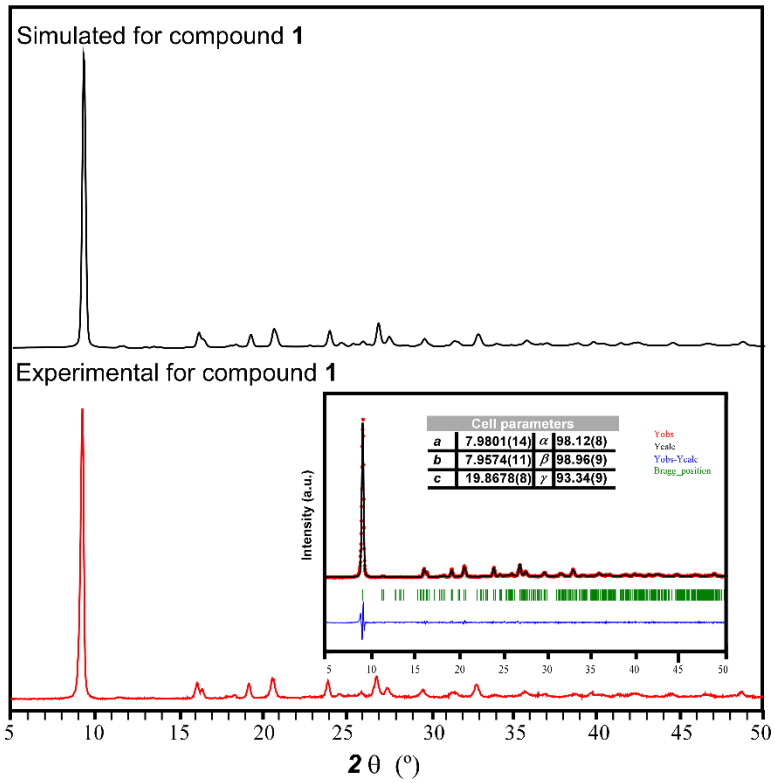


**Figure S3.** Comparison between the experimental PXRD data for compound **1** with that simulated from the crystal structure of **1**. Inset represents the pattern-matching analysis.

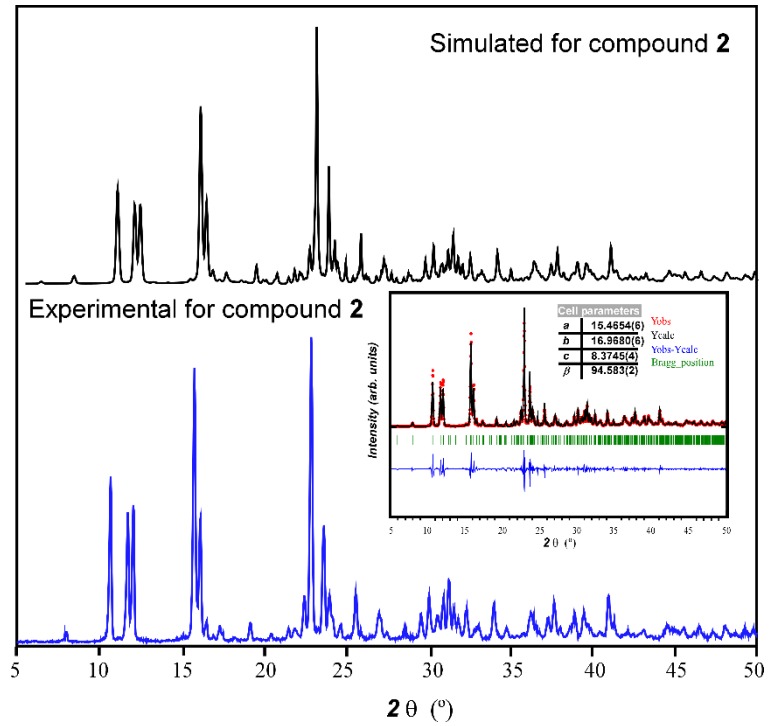


**Figure S4.** Comparison between the experimental PXRD data for compound **2** with that simulated from the crystal structure of **2**. Inset represents the pattern-matching analysis.

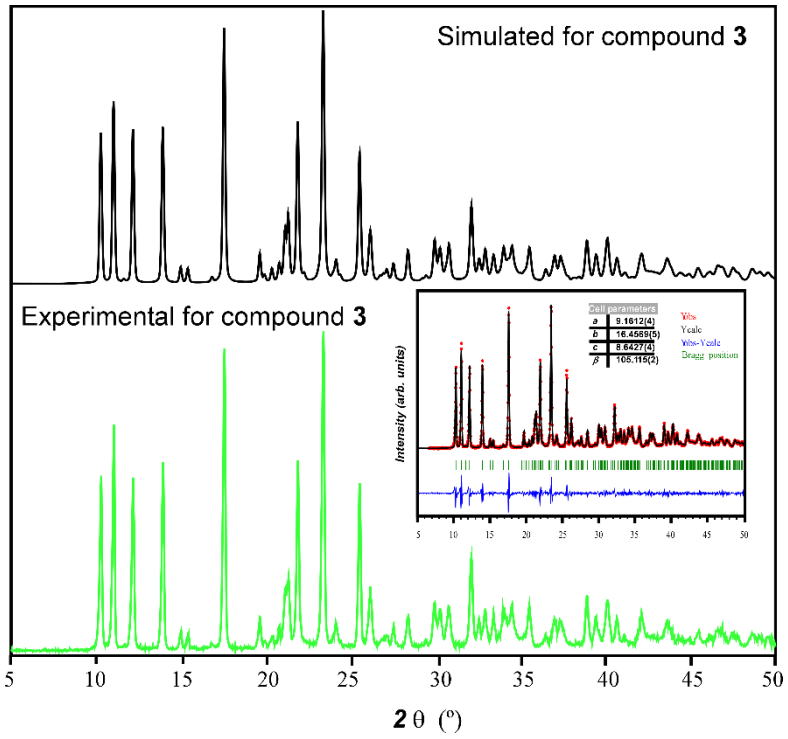


**Figure S5.** Comparison between the experimental PXRD data for compound **3** with that simulated from the crystal structure of **3**. Inset represents the pattern-matching analysis.

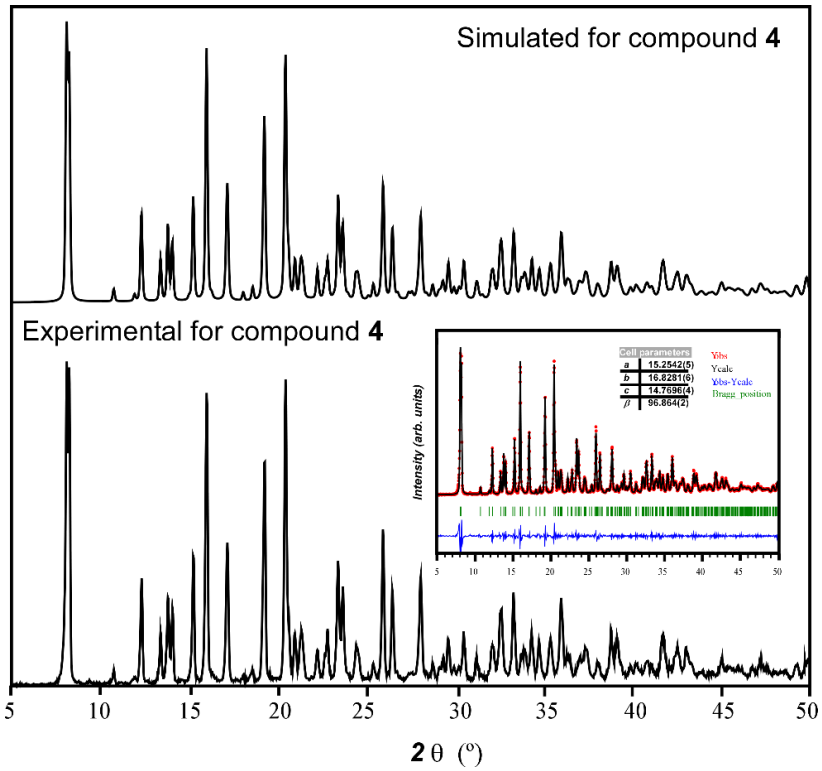


**Figure S6.** Comparison between the experimental PXRD data for compound **4** with that simulated from the crystal structure of **4**. Inset represents the pattern-matching analysis.

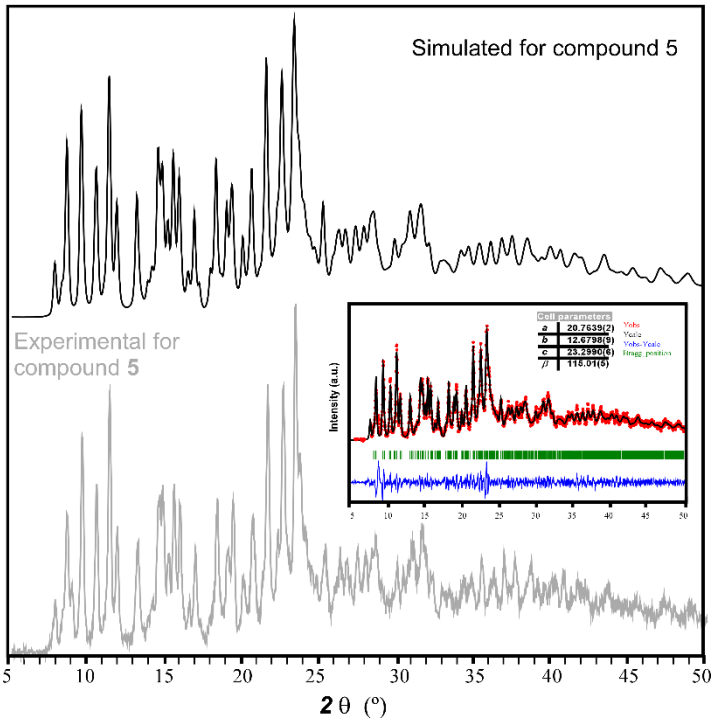


**Figure S7.** Comparison between the experimental PXRD data for compound **5** with that simulated from the crystal structure of **5**. Inset represents the pattern-matching analysis.

## S6. Structural details of compounds

**Table S8.** CShMs for the coordination environment of compounds **1, 2, 3, 4** and **5.**
Codes:

HP-6 1 D6h Hexagon

PPY-6 2 C5v Pentagonal pyramid

OC-6 3 Oh Octahedron

TPR-6 4 D3h Trigonal prism

JPPY-6 5 C5v Johnson pentagonal pyramid J2

| Structure [ML6] | HP-6 | PPY-6 | OC-6 | TPR-6 | JPPY-6 |
|---|---|---|---|---|---|
| **Comp. 1-Cd1** | 28.076 | 23.303 | **2.016** | 11.473 | 27.494 |
| **Comp. 1-Cd2** | 27.505 | 24.937 | **1.730** | 12.953 | 28.544 |
| **Comp. 2-Cd1** | 24.660 | 26.376 | **1.574** | 15.687 | 28.837 |
| **Comp. 2-Cd2** | 24.645 | 26.3802 | **1.568** | 15.693 | 28.850 |
| **Comp. 3** | 27.042 | 27.443 | **1.354** | 15.756 | 30.099 |
| **Comp. 4-Cd1** | 26.418 | 27.091 | **1.390** | 15.970 | 29.660 |
| **Comp. 4-Cd2** | 33.241 | 17.336 | 5.375 | **5.240** | 21.293 |
| **Comp. 5-Cd1** | 29.862 | 24.121 | **1.850** | 13.676 | 27.881 |
| **Comp. 5-Cd2** | 31.201 | 21.414 | **2.699** | 10.690 | 25.750 |

**Table S9.** Selected bond lengths for compound **1** (Å).[a]

| | | | |
|---|---|---|---|
| Cd1-O1A | 2.208(13) | Cd2-O1C | 2.238(13) |
| Cd1-O2B(i) | 2.517(13) | Cd2-O2D(iii) | 2.427(13) |
| Cd1-N1A | 2.300(16) | Cd2-N1C | 2.252(15) |
| Cd1-O1B | 2.266(13) | Cd2-O1D | 2.287(13) |
| Cd1-N1B | 2.239(15) | Cd2-N1D | 2.263(16) |
| Cd1-N61A(ii) | 2.501(16) | Cd1–N61C(iv) | 2.533(15) |

[a]Symmetry codes: (i) 3-x, 2-y, 2-z; (ii) 2-x, 2-y, 2-z; (iii) –x, -y, 1-z; (iv) –x, 1-y, 1-z.

**Table S10.** Structural parameters (Å, °) of hydrogen bond in compound **1.**

| *D–H···A*[a] | *D–H* | *H···A* | *D···A* | *D–H···A* |
|---|---|---|---|---|
| N61B–H61D···O2B(i) | 0.86 | 2.18 | 2.94(3) | 146.4 |
| N61D-H61H···O2D(ii) | 0.86 | 2.24 | 2.97(2) | 142.0 |

[a] D: donor. A: acceptor. Symmetry codes: (i) x, 1+y, z; (ii) -1+x, y, z.

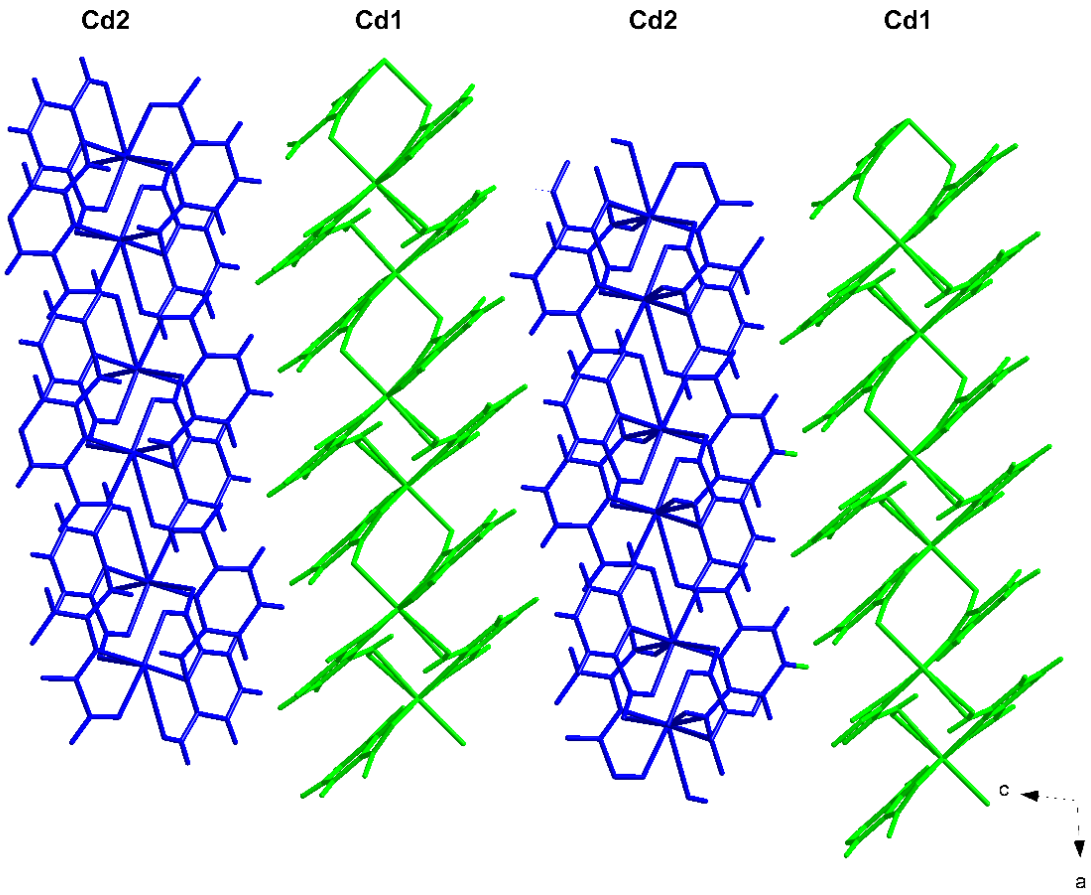


**Figure S8.** View of the packing of compound **1** showing the 2D supramolecular layers formed. Each layer is coloured differently for a better visualization.

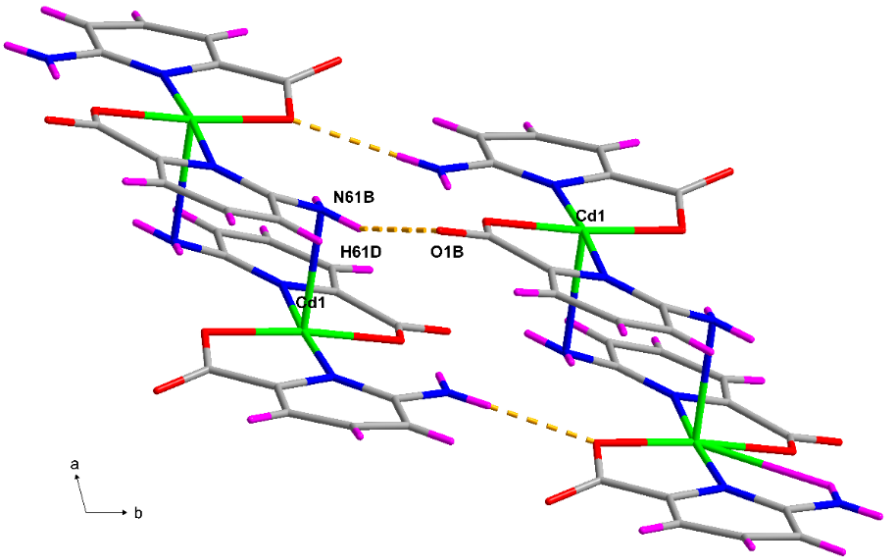


**Figure S9.** Established interlayer hydrogen bonds in compound **1**.

**Table S11.** Selected bond lengths for compound **2** (Å).[a]

| | | | |
|---|---|---|---|
| Cd1-N1A | 2.2635(15) | Cd2-N1B | 2.2739(16) |
| Cd1-N1A(i) | 2.2634(15) | Cd2-N1B(ii) | 2.2739(16) |
| Cd1-O1A | 2.2619(16) | Cd2-O1B | 2.2704(13) |
| Cd1-O1A(i) | 2.2619(16) | Cd2-O1B(ii) | 2.2704(13) |
| Cd1-N1C | 2.4540(17) | Cd2-N10C | 2.4275(17) |
| Cd1-N1C(i) | 2.4540(17) | Cd2-N10C(ii) | 2.4275(17) |

[a]Symmetry codes: (i) –x, -y, 1-z; (ii) 1-x, 1-y, 2-z.

**Table S12.** Structural parameters (Å, °) of hydrogen bonds in compound **2.**

| *D–H···A*[a] | *D–H* | *H···A* | *D···A* | *D–H···A* |
|---|---|---|---|---|
| N61A–H61B···O2B(i) | 0.88 | 2.07 | 2.879(2) | 151.8 |
| N61B-H61D···Ow(ii) | 0.88 | 2.00 | 2.876(3) | 176.2 |
| Ow-HwA···O2A(iii) | 0.85 | 1.94 | 2.790(2) | 173.1 |

[a] D: donor. A: acceptor. Symmetry codes: (i) -1+x, 1/2-y, -1/2+z; (ii) x, y, 1+z; (iii) x, 1/2-y, 1/2+z.

**Table S13.** Structural parameters (Å, °) of π-π interactions of compound **2.**[a]

| Ring···Ring[b] | α | DC | β | DZ |
|---|---|---|---|---|
| 1C–2C(i) | 24.22(8) | 4.0272(11) | 12.1 | 3.2464(7) |
| 2C–1C(ii) | 24.22(8) | 4.0272(11) | 36.3 | 3.9387(7) |

[a]Symmetry: (i) x, 1/2-y, -1/2+z; (ii) x, 1/2-y, 1/2+z. α: dihedral angle between mean planes of the rings (°), DC: distance between ring centroids (Å), β: angle between DC vector and normal to plane(I) (°), DZ: perpendicular distance of the centroids of the ring(I) on the plane of ring(II) (Å). [b] Rings: **1C**: N1C, C2C, C3C, C4C, C5C, C6C; **2C**: N10C, C9C, C8C, C7C, C12C, C11C.

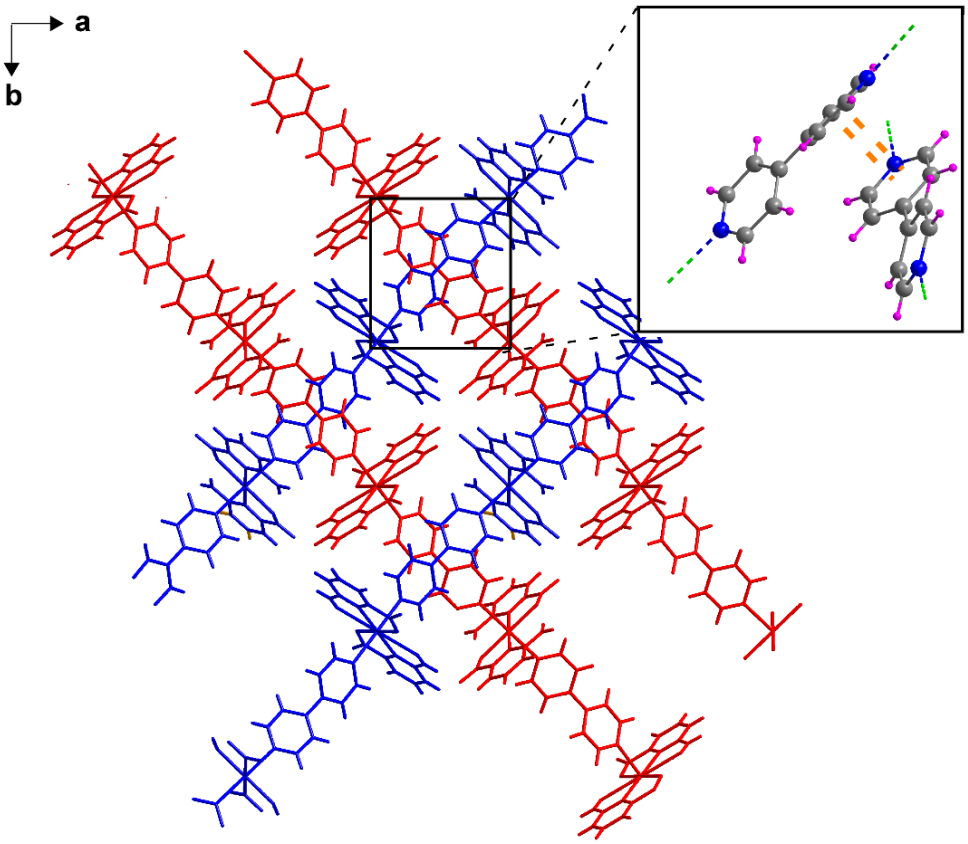


**Figure S10.** Packing of compound **2** showing the intersecting chains. Each colour represents each of the chains. Inset shows the established π-π stacking interactions between of 4,4´-bipyridine aromatic rings.

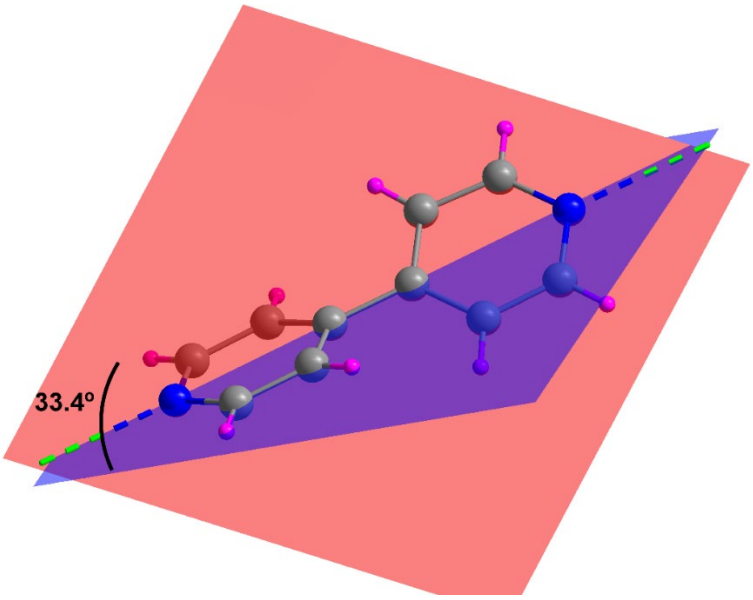


**Figure S11.** Twisted angle between the aromatic rings of a bridging bipy molecule in **2**.

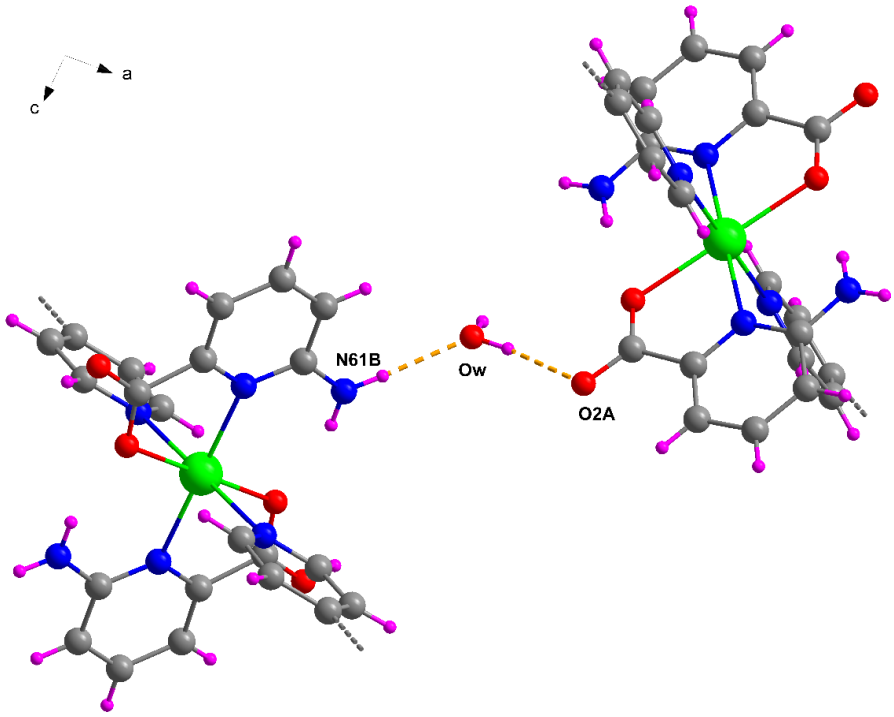


**Figure S12.** Image of compound **2** showing the interchain connections mediated by the lattice water molecule.

**Table S14.** Selected bond lengths for compound **3** (Å).[a]

| | | | |
|---|---|---|---|
| Cd1-O1A | 2.2678(12) | Cd1-N1A(i) | 2.3068(13) |
| Cd1-O1A(i) | 2.2679(12) | Cd1-N1B | 2.3741(18) |
| Cd1-N1A | 2.3068(13) | Cd1-N1B(i) | 2.3741(18) |

[a]Symmetry codes: (i) 1–x, –y, 1-z.

**Table S15.** Structural parameters (Å, °) of hydrogen bonds in compound **3.**

| *D–H···A*[a] | *D–H* | *H···A* | *D···A* | *D–H···A* |
|---|---|---|---|---|
| O1w-H11W···O2A | 0.85 | 2.08 | 2.919(3) | 169.1 |
| O1w-H12W···O2A(i) | 0.85 | 1.94 | 2.790(2) | 173.1 |
| N61B-H61B···O1w(ii) | 0.86 | 2.16 | 2.978(4) | 157.7 |

[a] D: donor. A: acceptor. Symmetry codes: (i) x, -3/2-y, -1/2+z; (ii) -1+x, -3/2-y, -1/2+z.

**Table S16.** Structural parameters (Å, °) of π-π interactions of compound **3.**[a]

| Ring···Ring[b] | α | DC | β | DZ |
|---|---|---|---|---|
| 1A–1A(i) | 4.62(17) | 4.4140(3) | 35.5 | 3.5911(15) |

[a]Symmetry: (i) x, 1/2-y, -1/2+z. α: dihedral angle between mean planes of the rings (°), DC: distance between ring centroids (Å), β: angle between DC vector and normal to plane(I) (°), DZ: perpendicular distance of the centroids of the ring(I) on the plane of ring(II) (Å). [b] Rings: **1A**: N1A, C2A, C3A, C4A, C5A, C6A.

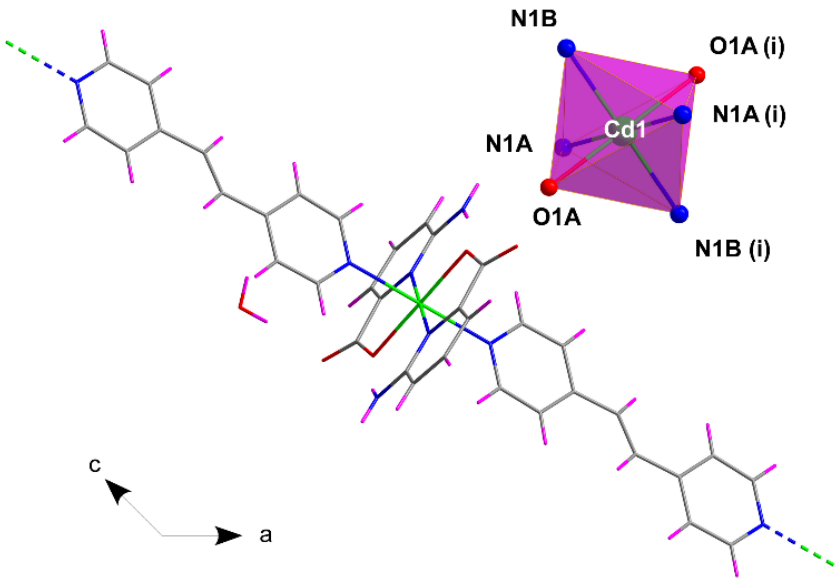


**Figure S13.** Fragment of a single-chain of compound **3** with the coordination polyhedra. Color code: C = grey, H = pink, Cd = green, N = blue, O = red.

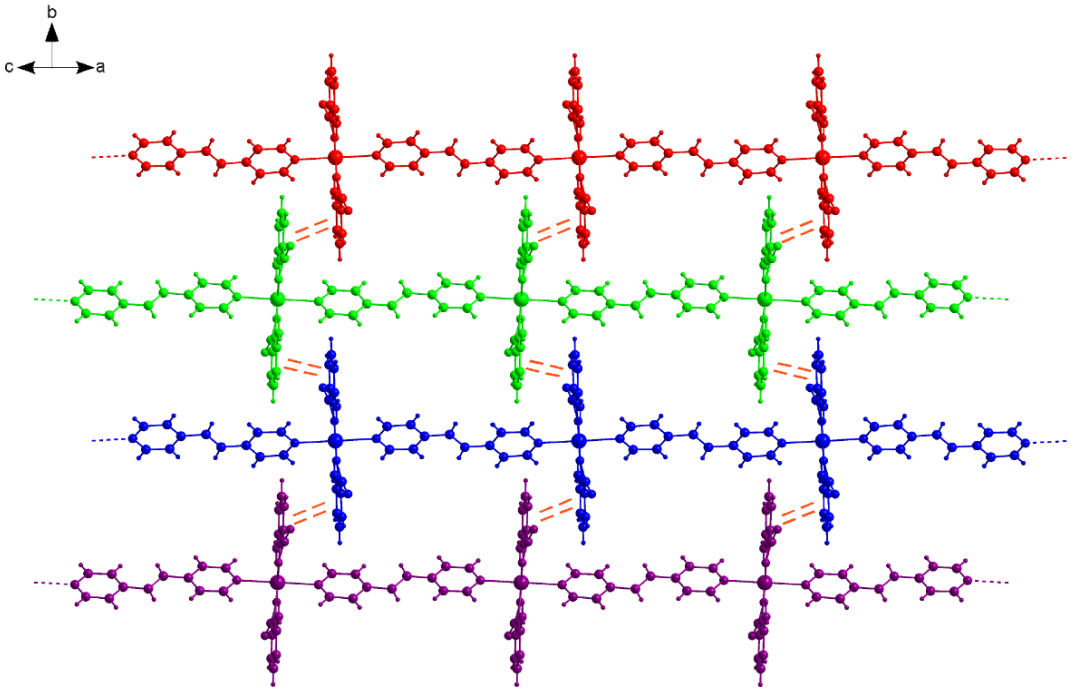


**Figure S14.** Rods of compound **3** stacked by π-π interactions between 6apic molecules.

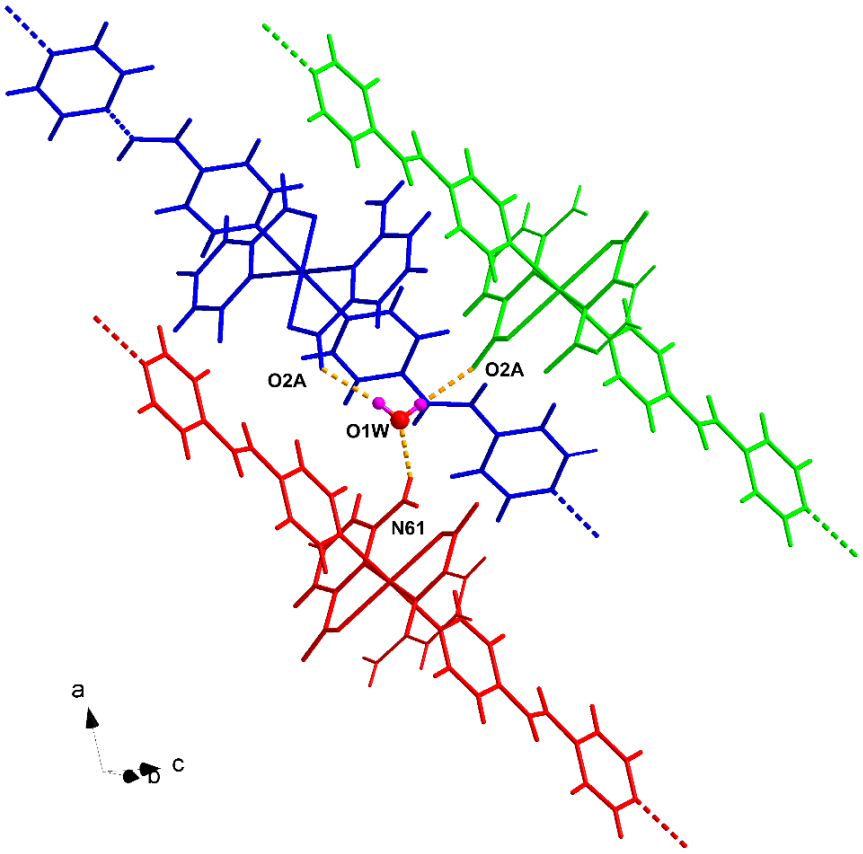


**Figure S15.** Connectivity between chains in compound **3** by the lattice water molecule by hydrogen-bonds.

**Table S17.** Selected bond lengths for compound **4** (Å).[a]

| | | | |
|---|---|---|---|
| Cd1-N1B | 2.2969(17) | Cd2-N1A | 2.2923(16) |
| Cd1-N1B(i) | 2.2969(17) | Cd2-N1A(ii) | 2.2924(16) |
| Cd1-O1B | 2.2680(14) | Cd2-O1A | 2.3129(15) |
| Cd1-O1B(i) | 2.2679(14) | Cd2-O1A(ii) | 2.3129(15) |
| Cd1-N1C | 2.4460(18) | Cd2-O2B | 2.2802(15) |
| Cd1-N1C(i) | 2.4460(18) | Cd2-O2B(ii) | 2.2802(15) |

[a]Symmetry codes: (i) 1–x, -1-y, 1-z; (ii) 1-x, y, 1/2-z.

**Table S18.** Structural parameters (Å, °) of hydrogen bonds in compound **4.**

| *D–H···A*[a] | *D–H* | *H···A* | *D···A* | *D–H···A* |
|---|---|---|---|---|
| N61A-H61A···O2B | 0.86 | 2.06 | 2.891(2) | 162.0 |
| N61B-H61D···O2A(i) | 0.86 | 2.07 | 2.862(2) | 152.9 |

[a] D: donor. A: acceptor. Symmetry codes: (i) -1/2+x, -1/2+y, 1/2+z.

**Table S19.** Structural parameters (Å, °) of π-π interactions of compound **4.**[a]

| Ring···Ring[b] | α | DC | β | DZ |
|---|---|---|---|---|
| 1A–1B(i) | 10.70(10) | 3.7009(12) | 25.8 | 3.3319(8) |
| 1B-1A(i) | 10.70(10) | 3.7009(12) | 22.4 | 3.4218(8) |
| 1C-1C(ii) | 9.24(10) | 3.7305(12) | 8.4 | 3.6906(9) |

[a]Symmetry: (i) 1/2-x, 1/2-y, 1/2-z; (ii) 3/2-x, y, 1-z. α: dihedral angle between mean planes of the rings (°), DC: distance between ring centroids (Å), β: angle between DC vector and normal to plane(I) (°), DZ: perpendicular distance of the centroids of the ring(I) on the plane of ring(II) (Å). [b] Rings: **1A**: N1A, C2A, C3A, C4A, C5A, C6A; **1B**: N1B, C2B, C3B, C4B, C5B, C6B; **1C**: N1C, C2C, C3C, C4C, C5C, C5C.

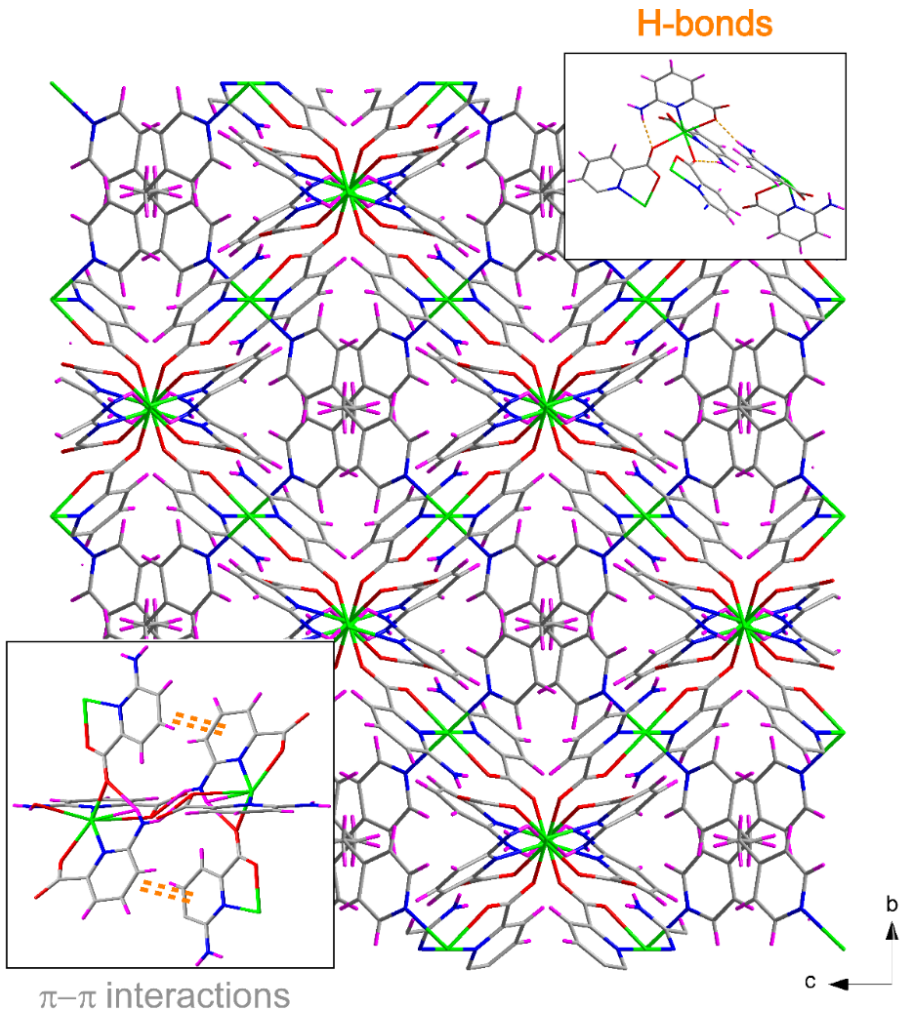


**Figure S16.** View down the *a* axis of compound **4** showing the efficient 3D packing sustained by π-π and hydrogen bonding interactions. Insets provides a better view of the interactions that give rise to such efficient packing.

**Table S20.** Selected bond lengths for compound **5** (Å).[a]

| | | | |
|---|---|---|---|
| Cd1-N1A | 2.312(5) | Cd2-N1D | 2.371(5) |
| Cd1-O1A | 2.333(4) | Cd2-O1D | 2.273(4) |
| Cd1-N1B | 2.368(4) | Cd2-N1E | 2.325(4) |
| Cd1-O1B | 2.282(4) | Cd2-O1E | 2.327(4) |
| Cd1-N1C | 2.301(5) | Cd2-N1F | 2.311(5) |
| Cd1-N13C(i) | 2.330(5) | Cd2-N13F(ii) | 2.344(4) |

[a]Symmetry codes: (i) x. -1+y, z; (ii) x, -1/2-y, 1/2-z.

**Table S21.** Structural parameters (Å, °) of hydrogen bonds in compound **5.**

| *D–H···A*[a] | *D–H* | *H···A* | *D···A* | *D–H···A* |
|---|---|---|---|---|
| N61A-H61B···O6w(i) | 0.86 | 2.01 | 2.869(6) | 175.4 |
| N61B-H61D···O5w(ii) | 0.86 | 2.09 | 2.894(7) | 155.1 |
| N61D-H61F···O1w(iii) | 0.86 | 2.01 | 2.867(6) | 174.6 |
| N61E-H61H···O2w(iv) | 0.86 | 2.04 | 2.873(6) | 163.3 |
| O1w-H1wA···O3w | 0.86 | 1.98 | 2.799(6) | 157.7 |
| O1w-H1wB···O1w | 0.86 | 2.00 | 2.856(5) | 172.7 |
| O2w-H2wA···O3w | 0.85 | 2.00 | 2.837(6) | 165.5 |
| O3w-H3wA···O2A | 0.86 | 1.95 | 2.795(5) | 169.7 |
| O3w-H3wB···O2D(v) | 0.85 | 1.98 | 2.829(6) | 175.4 |
| O5w-H5wA···O4w | 0.88 | 2.00 | 2.842(6) | 159.2 |
| O5w-H5wB···O6w | 0.86 | 1.94 | 2.768(6) | 160.6 |
| O6w-H6wA···O7w | 0.85 | 1.84 | 2.681(6) | 169.6 |
| O6w-H6wB···O2B | 0.85 | 1.91 | 2.727(6) | 161.8 |
| O7w-H7wA···O2A(iii) | 0.86 | 1.96 | 2.797(7) | 164.0 |
| O7w-H7wB···O2E | 0.85 | 1.96 | 2.781(6) | 160.6 |

[a] D: donor. A: acceptor. Symmetry codes: (i) 1-x, -1/2+y, 1/2-z; (ii) x, 1/2-y, -1/2+z; (iii) x, 1/2-y, 1/2+z; (iv) 2-x, -1/2+y, 1/2-z; (v) x, -1/2-y, -1/2+z.

**Table S22.** Structural parameters (Å, °) of π-π interactions in compound **5.**

| Ring···Ring[b] | α | DC | β | DZ |
|---|---|---|---|---|
| 1A–1A(i) | 0.0(3) | 3.933(4) | 29.5 | 3.424(2) |
| 1E-1E(ii) | 0.0(3) | 3.491(4) | 8.422.5 | 3.225(2) |

[a]Symmetry: (i) 1-x, -y, -z; (ii) 2-x, -y, 1-z. α: dihedral angle between mean planes of the rings (°), DC: distance between ring centroids (Å), β: angle between DC vector and normal to plane(I) (°), DZ: perpendicular distance of the centroids of the ring(I) on the plane of ring(II) (Å). [b] Rings: **1A**: N1A, C2A, C3A, C4A, C5A, C6A; **1E**: N1E, C2E, C3E, C4E, C5E, C6E.

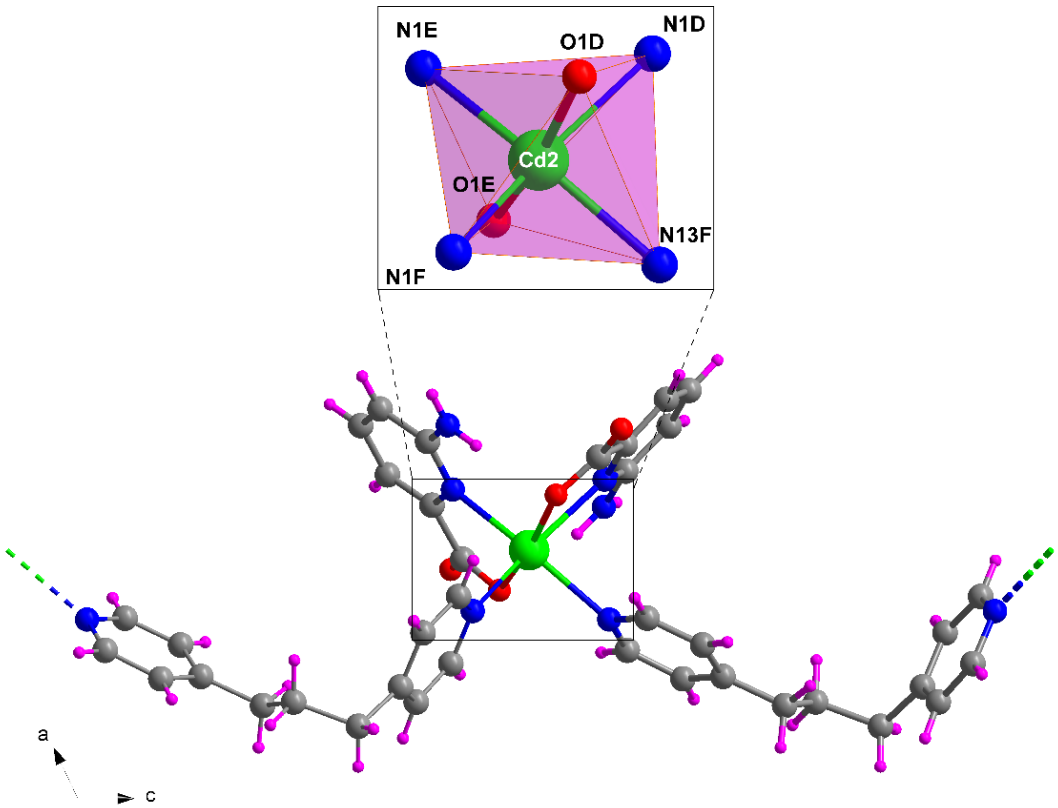


**Figure S17.** Fragment of the structure of compound **5** that shows the second equivalent chain together with the coordination polyhedron.

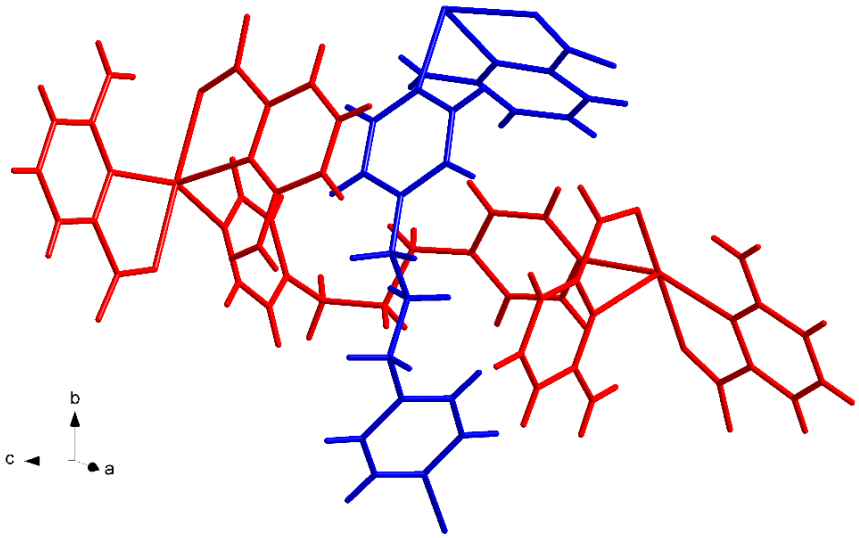


**Figure S18.** View of two intersecting chains in compound **5**.

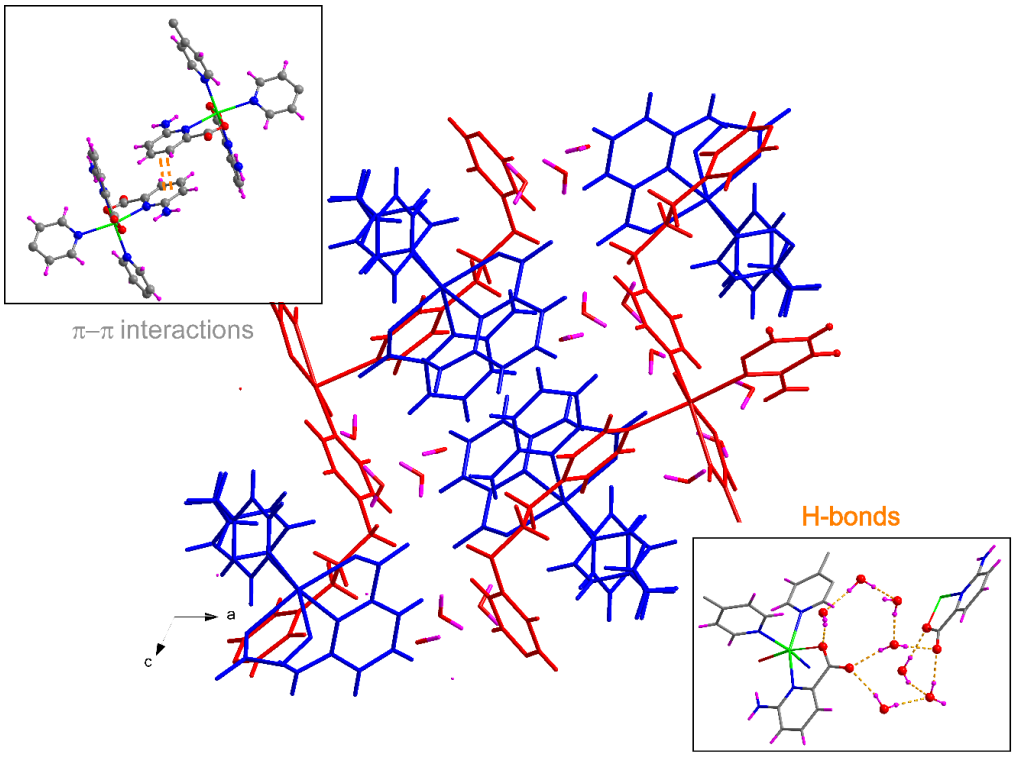


**Figure S19.** Packing of compound **5** hold by π-π stacking interactions and the hydrogen-bonding network established by the lattice water molecules. Insets show a better view of the π-π stacking interactions and the hydrogen-bonding network.

## S7. Photoluminescent measurements

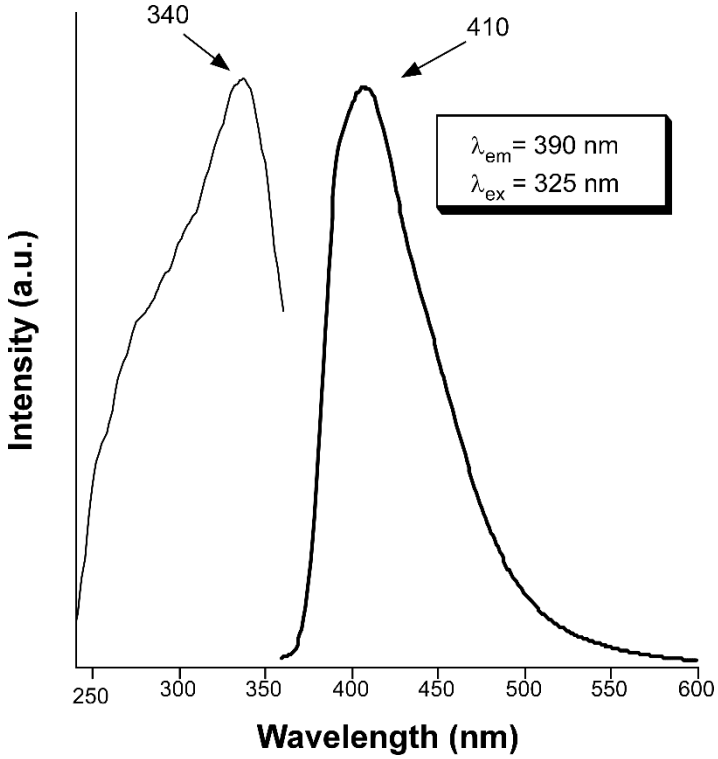


**Figure S20.** Excitation and emission spectra of H6apic recorded at room temperature.

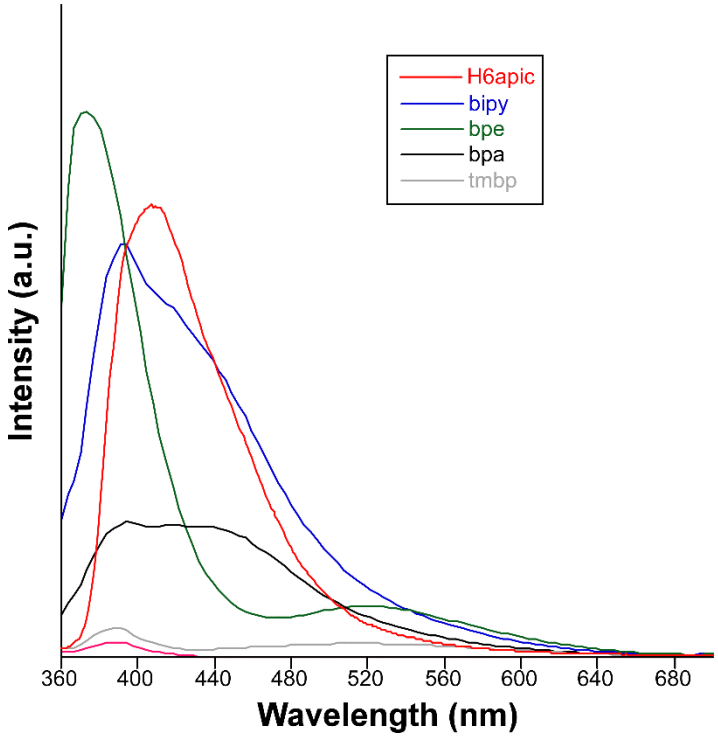


**Figure S21.** Emission spectra of free H6apic and bipyridyl co-linkers employed for the construction of the CPs at room temperature ($\lambda_{ex}$ = 325 nm).

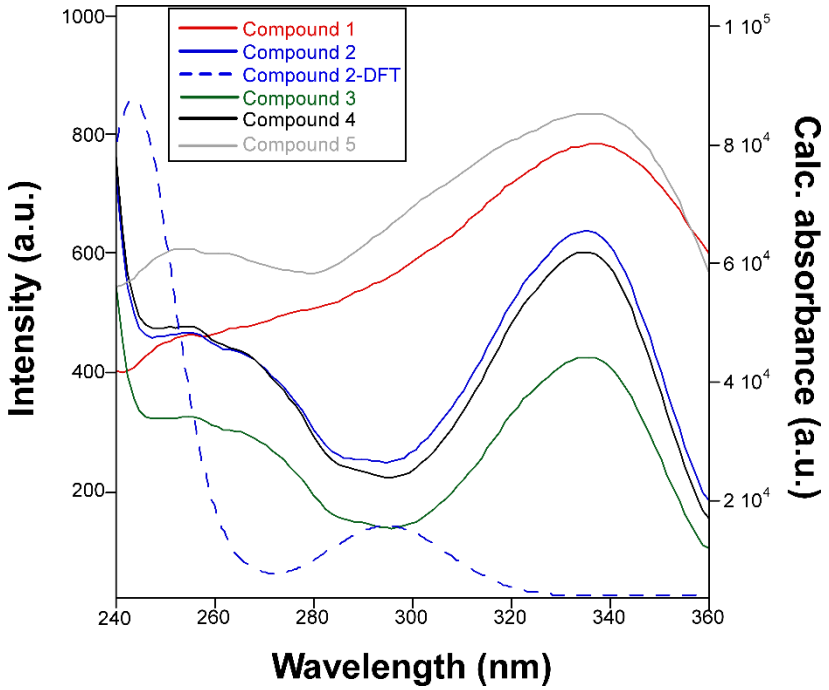


**Figure S22.** Excitation spectra compounds **1**-**5** monitored at room temperature ($\lambda_{em}$ = 390 nm) together with the calculated excitation for the model of compound **2**.

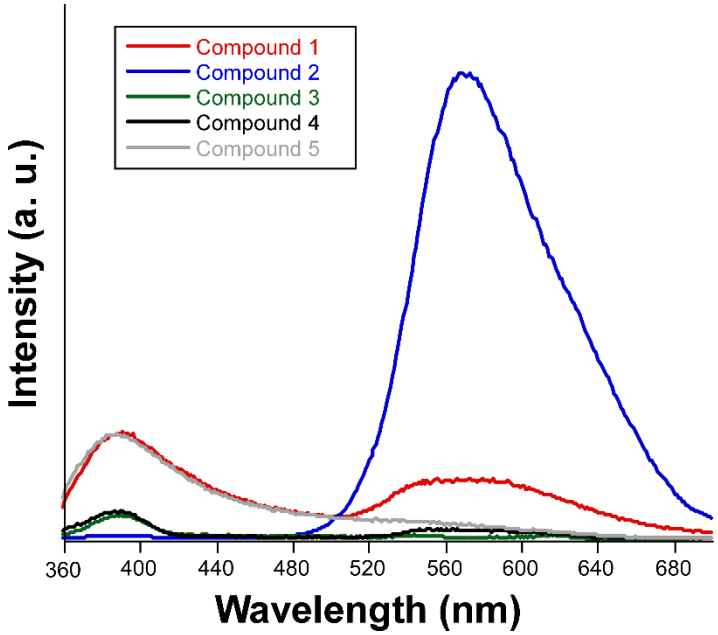


**Figure S23.** Delayed-emission spectra of compound **1**-**5** recorded at room temperature ($\lambda_{ex}$ = 325 nm).

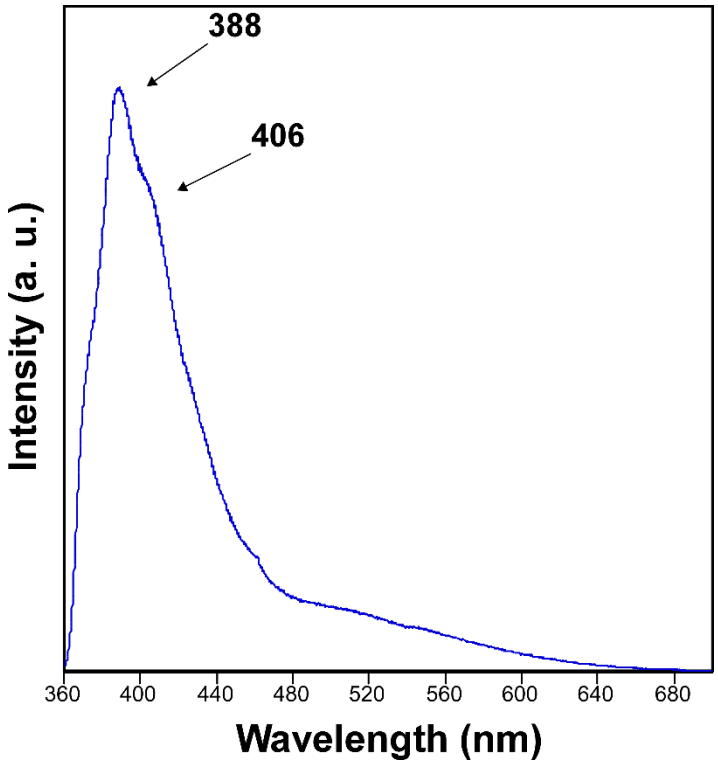


**Figure S24.** Emission spectra of compound **2** at 10 K excited with a laser at 325 nm.

At this temperature, 10 K, decay curves were collected at two representative wavelengths of the fluorescence and phosphorescence of the sample. The first measurement was performed at 408 nm and not at 388 nm (the most intense maximum of the main band) due to its proximity to the excitation source wavelength (370 nm, a pulsed laser diode).

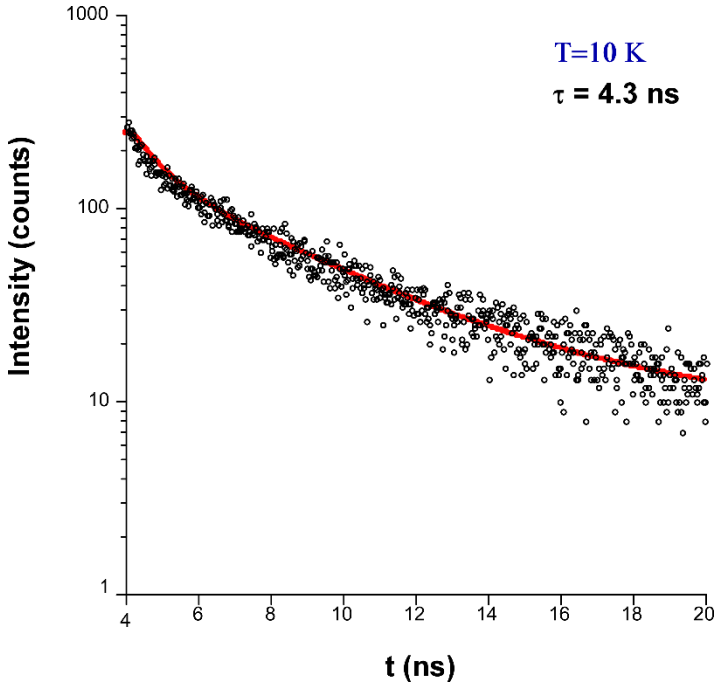


**Figure S25.** Decay curve of compound **2** recorded at an emission wavelength of 406 nm excited at 370 nm.

**Table S23.** Best fit results of decay curves of compound **2** measured at an emission wavelength of 406 nm.

| Temperature (K) | $\tau_1$ (ns) | $\tau_2$ (ns) | Chi Sq. |
|---|---|---|---|
| 298 | 0.3(3) / 16.0% | 3.5(1) / 84% | 1.252 |

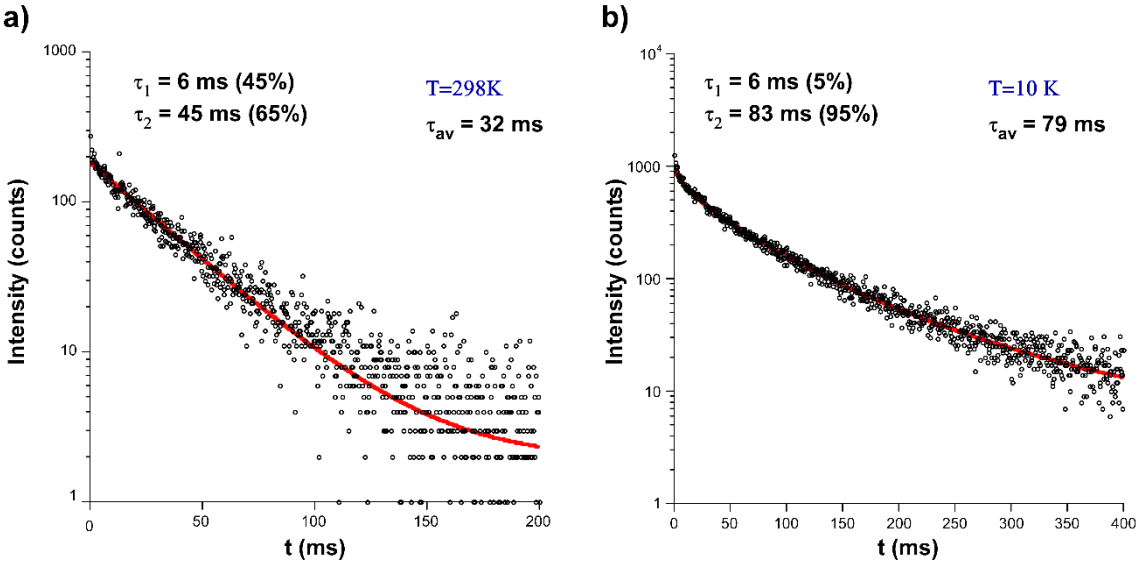


**Figure S26.** Decay curves of compound **2** recorded at an emission wavelength of 560 nm excited at 325 nm at (a) room temperature and (b) 10 K.

**Table S24.** Best fit results of decay curves of compound **2** measured at an emission wavelength of 560 nm.

| Temperature (K) | $\tau_1$ (ms) | $\tau_2$ (ms) | Chi Sq. |
|---|---|---|---|
| 298 | 6.1(1) / 45% | 45.1(1) / 65% | 1.397 |
| 10 | 5.8(1) / 5% | 82.7(1) / 95% | 1.282 |

## S8. DFT calculations

The main excitation energies have calculated by means of TD-DFT calculations on the optimized model consisting of the monomeric complex cut from compound **2** and the simulated spectrum has been compared with the diffuse reflectance spectrum in order to guess the mechanism followed during the photoluminescence process.

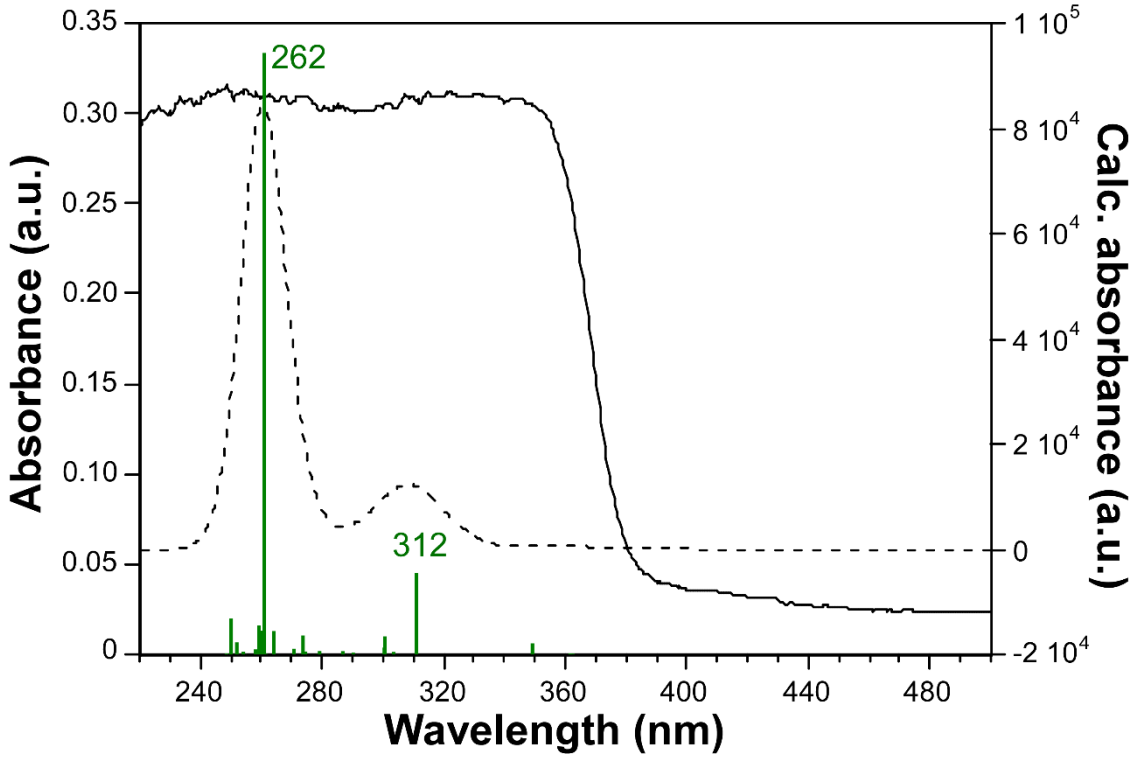


**Figure S27.** Diffuse reflectance (solid line) and TD-DFT computed absorption (dotted line) spectra of compound **2** showing the most relevant excitation lines.

Taking into account that the diffuse reflectance spectrum shows a wide band covering the 220-380 nm range in which two different bands can be guessed, which peak at similar wavelengths to those shown in the excitation spectrum of the compound. The calculated bands, slightly blue-shifted with respect to the experimental ones, have been used for the interpretation of the photoluminescence process.

**Table S25.** Experimental (diffuse reflectance) and calculated main excitation wavelengths (nm). Singlet electronic transitions and associated oscillator strengths were calculated using a model of compound **2** in gas phase**.**

| Exp. λ | Calc λ | Significant contributions | State | Osc. st. (a.u.) |
|---|---|---|---|---|
| 330 | 312 | HOMO → LUMO + 2 (84%) | 12 | 0.1343 |
| 250 | 262 | HOMO – 13 → LUMO (43%)<br>HOMO – 14 → LUMO + 1 (43%) | 51 | 0.9825 |

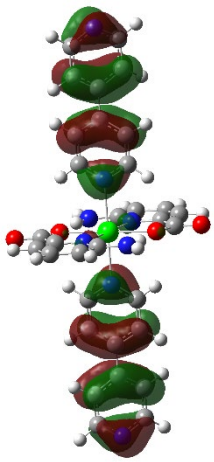

HOMO – 14

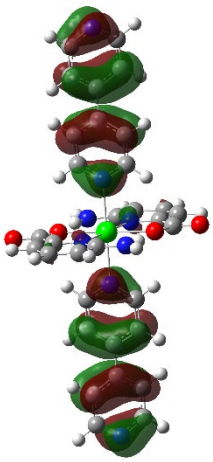

HOMO – 13

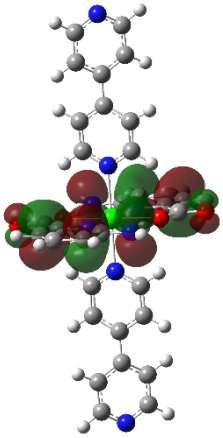

HOMO – 1

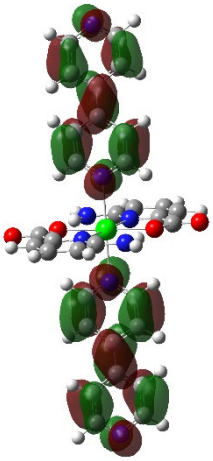

LUMO

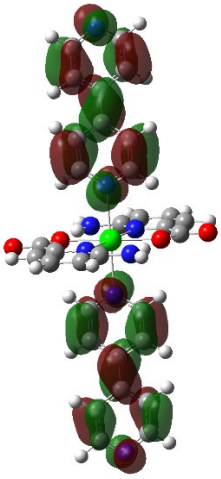

LUMO + 1

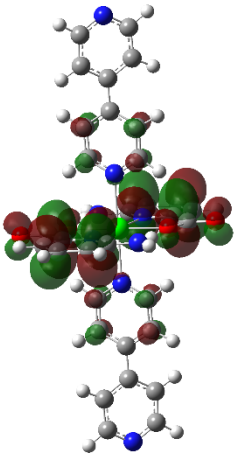

LUMO + 2

**Figure S28.** Highest Occupied and Lowest Unoccupied Molecular Orbitals involved in the singlet excitations of a suitable model of compound **2** .

**Table S26.** Experimental and calculated main excitation wavelengths (nm) at 10 K. Singlet electronic transitions and associated oscillator strengths were calculated using a model of compound **3** in gas phase**.**

| Exp. λ | Calc λ | Significant contributions | State | Osc. st. (a.u.) |
|---|---|---|---|---|
| 338 | 314 | HOMO – 5 → LUMO + 1 (42%)<br>HOMO – 4 → LUMO (55%) | 15 | 2.1458 |

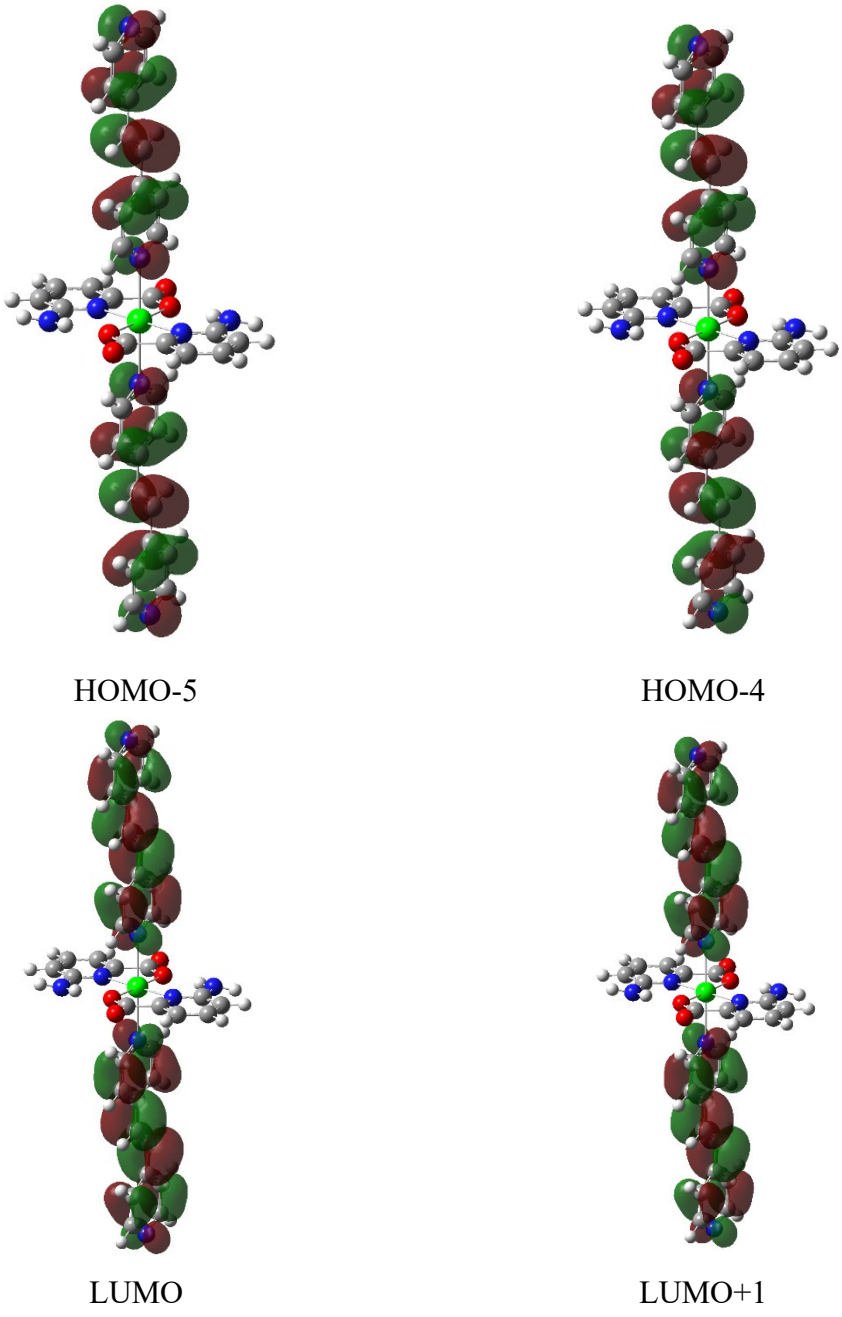


**Figure S29.** Highest Occupied and Lowest Unoccupied Molecular Orbitals in compound **3** involved in the single excitation charge transitions.

**Table S27.** Experimental and calculated main emission wavelengths (nm) at 10 K. Singlet electronic transitions and associated oscillator strengths were calculated using a model of compound **3** in gas phase**.**

| Exp. λ | Calc λ | Significant contributions | Osc. st. (a.u.) |
|---|---|---|---|
| 391 | 343 | HOMO – 4 → LUMO (95%)<br>HOMO – 8 → LUMO (3%) | 1.2726 |
| | 353 | HOMO – 5 → LUMO (97%) | 1.3671 |

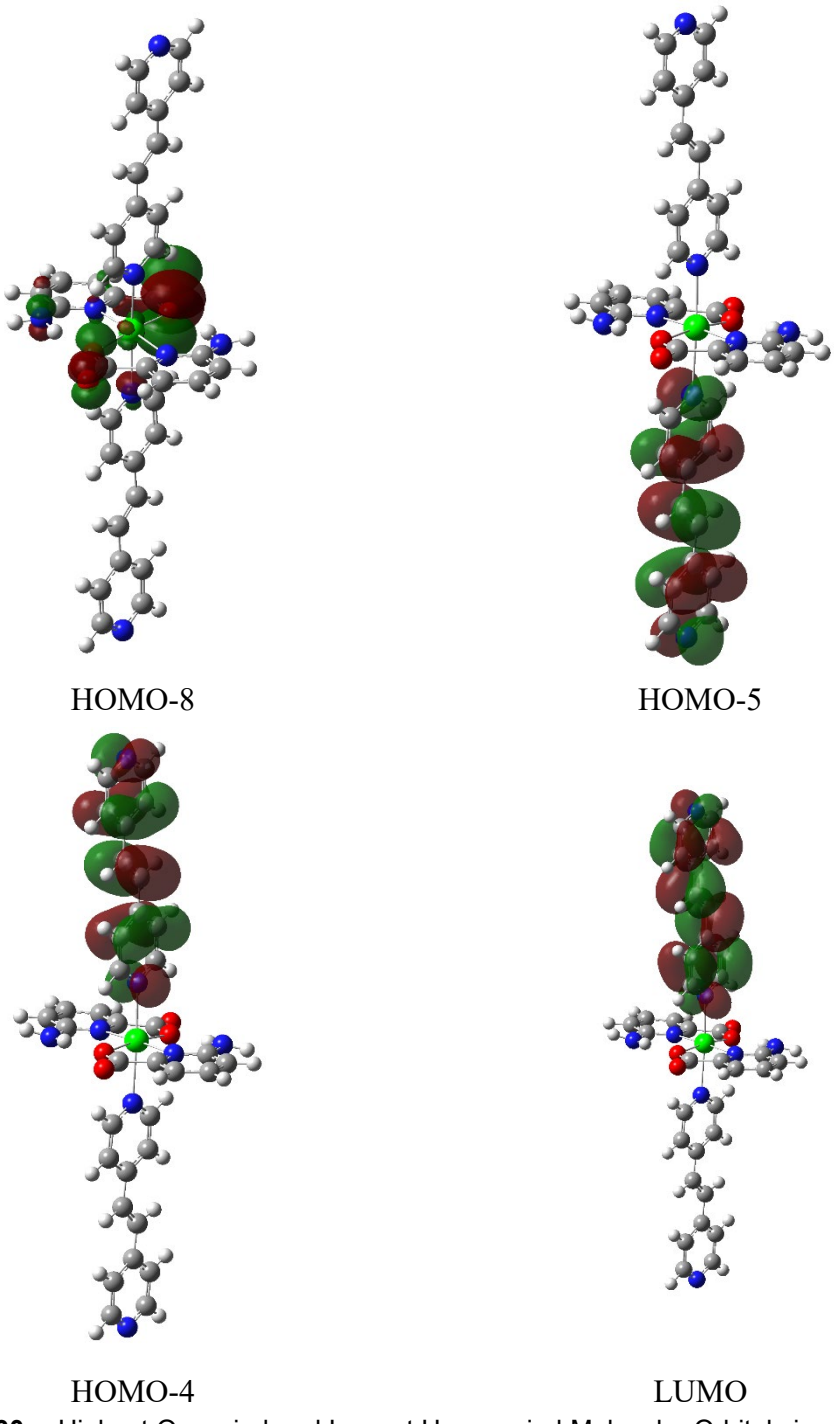


**Figure S30.** Highest Occupied and Lowest Unoccupied Molecular Orbitals in compound **3** involved in the single emission charge transitions.

## S9. Sensing experiments

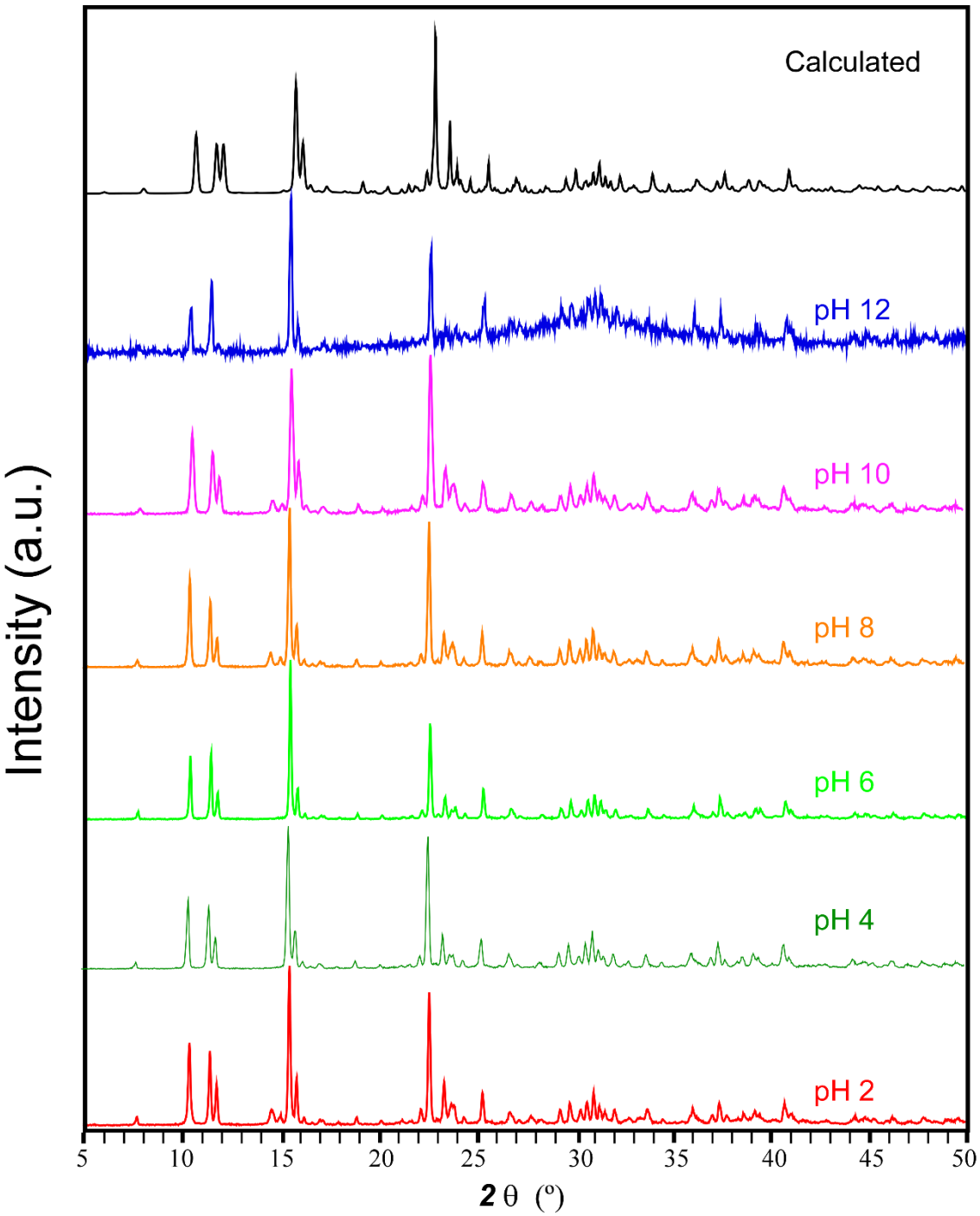


**Figure S31.** Comparative PXRD diffractograms acquired for the recovered solid of compound **2** from aqueous solutions at variable pH to confirm the stability.

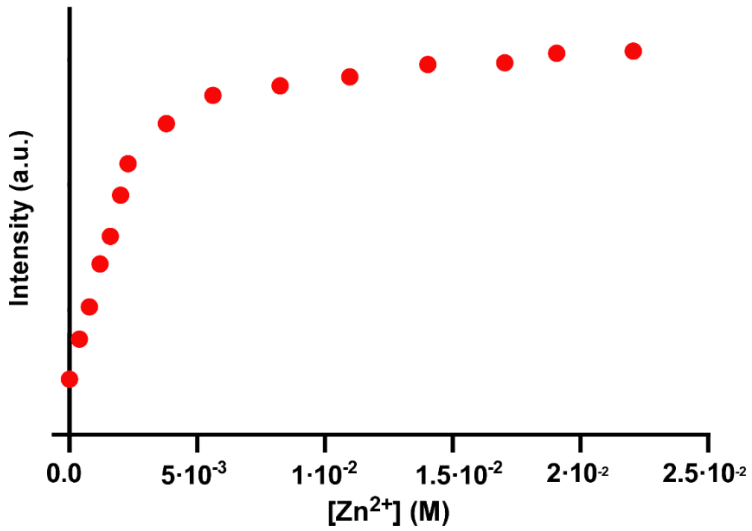


**Figure S32.** Fluorescent intensity of compound **2** at an emission wavelength of 393 nm dispersed in water according to different concentrations of $Zn^{2+}$ ion ($\lambda_{ex}$ = 340 nm).

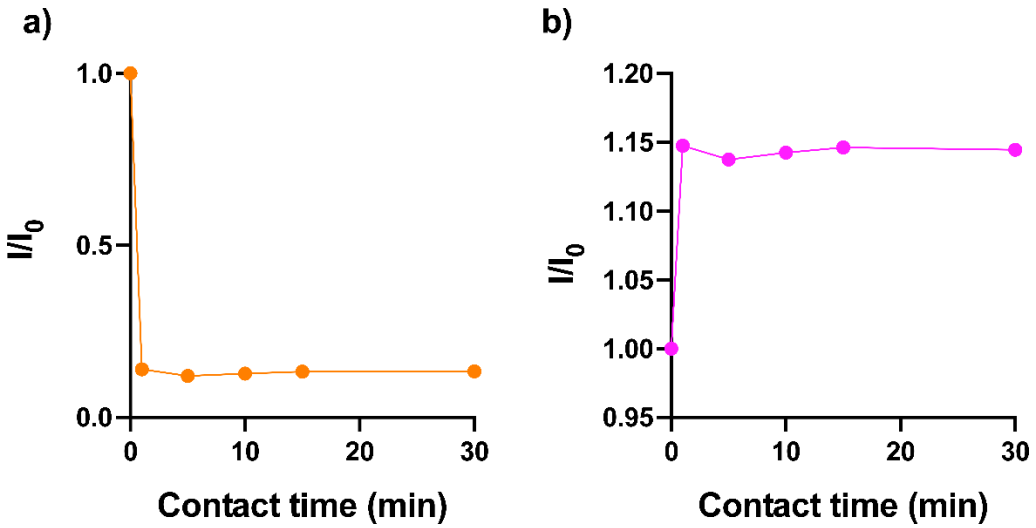


**Figure S33.** Comparative photoluminescence data for the water dispersed samples of compound **2** with and without metal ions in the form of: **a)** excitation and **b)** emission spectra.

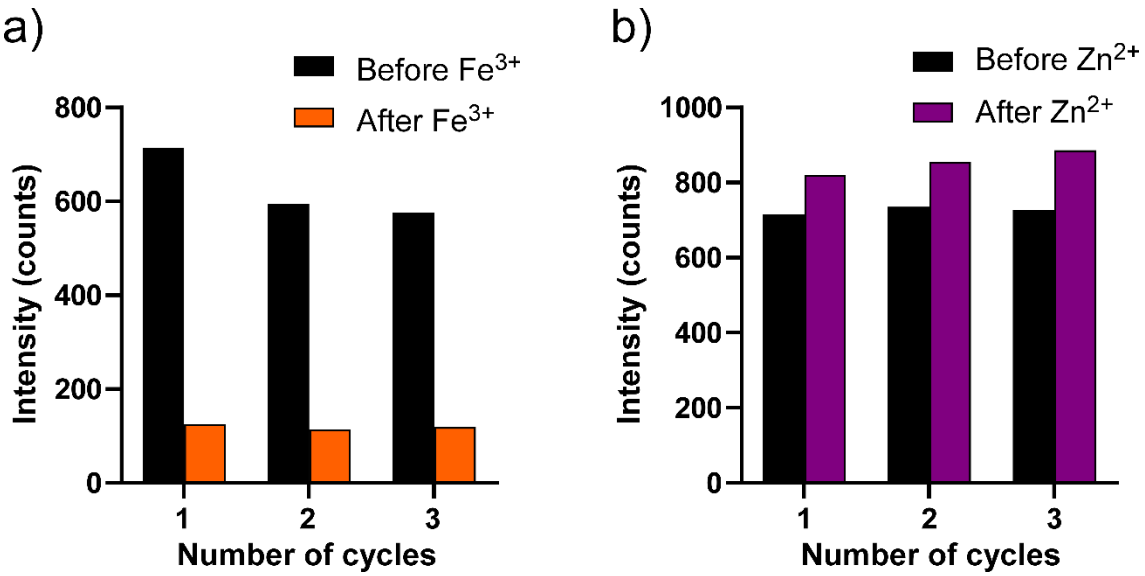


**Figure S34.** Plots showing the intensity of the main PL emission band ($\lambda_{em}$ = 340 nm) of compound **2** before and after each soaking in the corresponding aqueous solution (left: $Fe^{3+}$(aq) and right: $Zn^{2+}$(aq)) during three consecutive cycles.

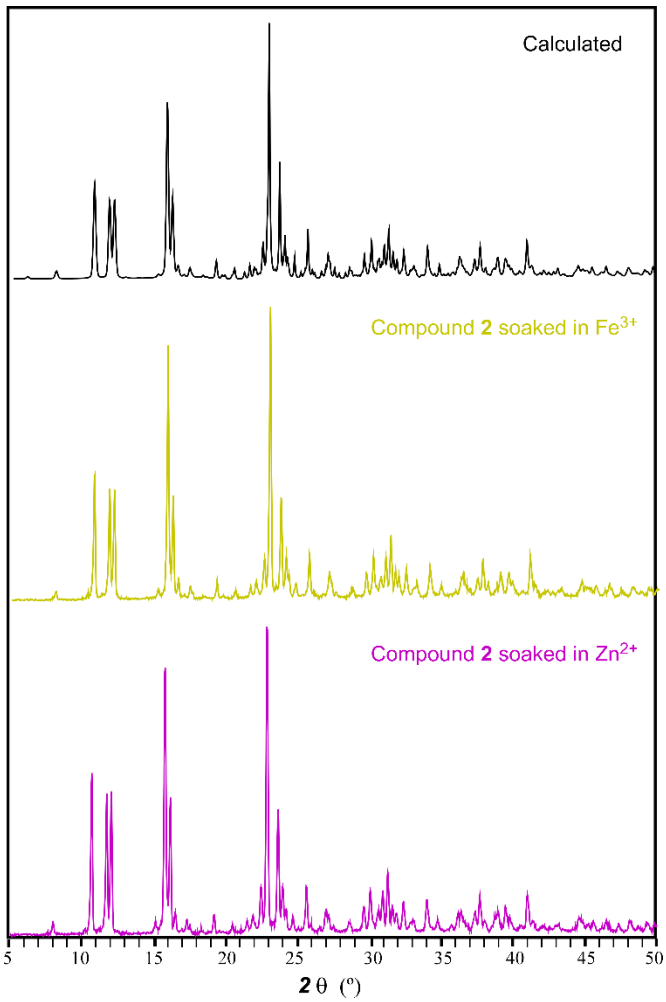


**Figure S35.** Diffraction patterns of compound **2** after being soaked for 24 hours in aqueous solutions containing $Fe^{3+}$ (yellow) and $Zn^{2+}$ (purple).

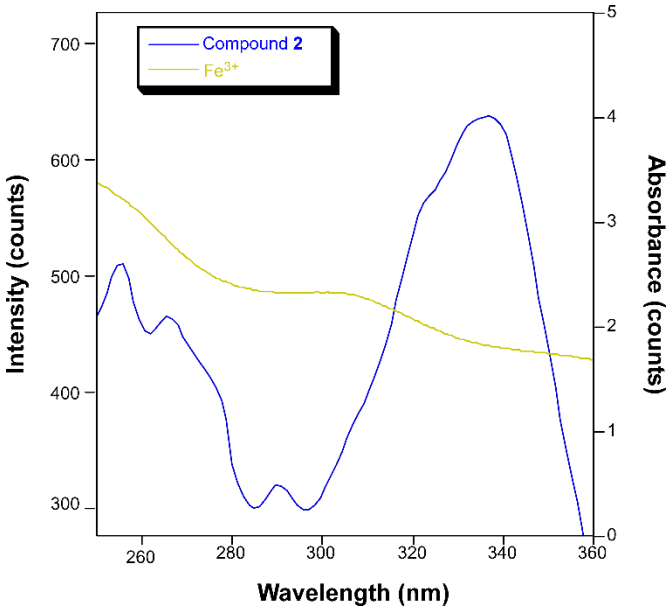


**Figure S36.** Simultaneous representation of absorbance spectrum of $Fe^{3+}$ aqueous solution (yellow) and excitation spectrum of compound **2** ($\lambda_{em}$ = 390 nm) (blue).

In order to further study the $Fe^{3+}$ and $Zn^{2+}$ sensing performance of compound **2**, the photoluminescence excitation and emission spectra were measured with the same experimental setup, finding that the interaction with these target ions does not affect the excitation and emission bands:

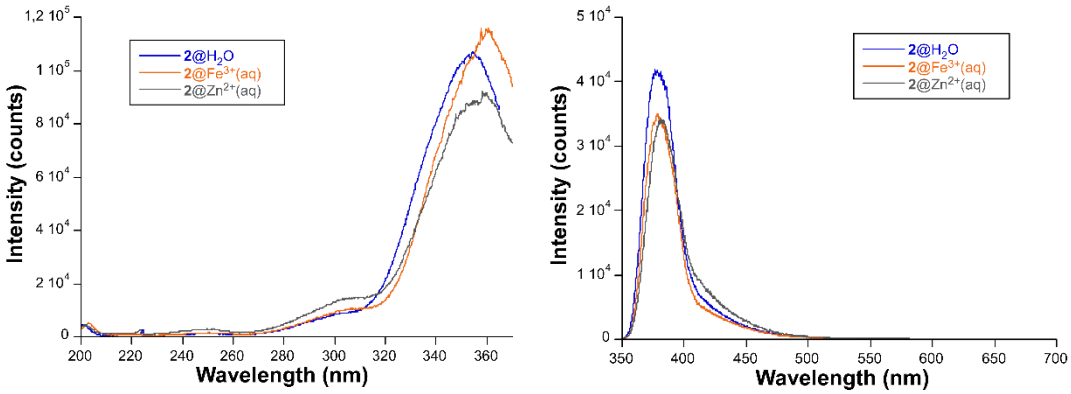


**Figure S37.** Comparative photoluminescence data for the water dispersed samples of compound **2** with and without metal ions in the form of: **a)** excitation and **b)** emission spectra.

However, the presence of these ion brings a notable effect in the emission lifetime. Although the signal is composed of two well distinguished components (with a live difference of one order of magnitude) in the logarithmic plots and this nature is kept in the presence analytes, the weights of these components clearly vary for the sensor during the detection. On the one hand, the quenching of $Fe^{3+}$ ion on compound **2** promotes a decrease of the long-lived component bringing an overall increase of the lifetime. On the other hand, the addition of $Zn^{2+}$ ion to the dispersion generates a substantial enlargement of the lifetime. This behaviour is in agreement with trends observed during the titration experiments.

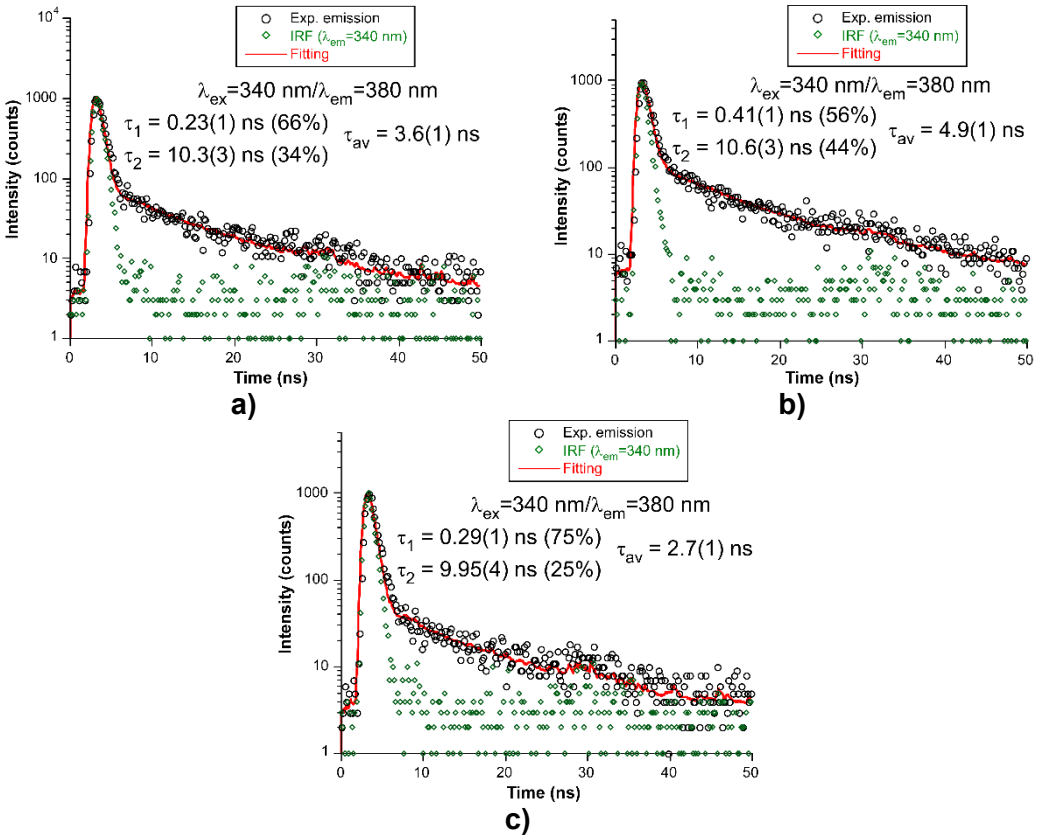


**Figure S38.** Decay curves of water dispersions of compound **2** (**2**@$H_2O$) recorded at $\lambda_{em}$ = 380 nm and $\lambda_{ex}$ = 340 nm room temperature for: **a)** blank (metal ion free) dispersion, **b)** $Zn^{2+}$-containing dispersion (**2**@$Zn^{2+}$(aq) and **c)** $Fe^{3+}$-containing dispersion (**2**@$Fe^{3+}$(aq).

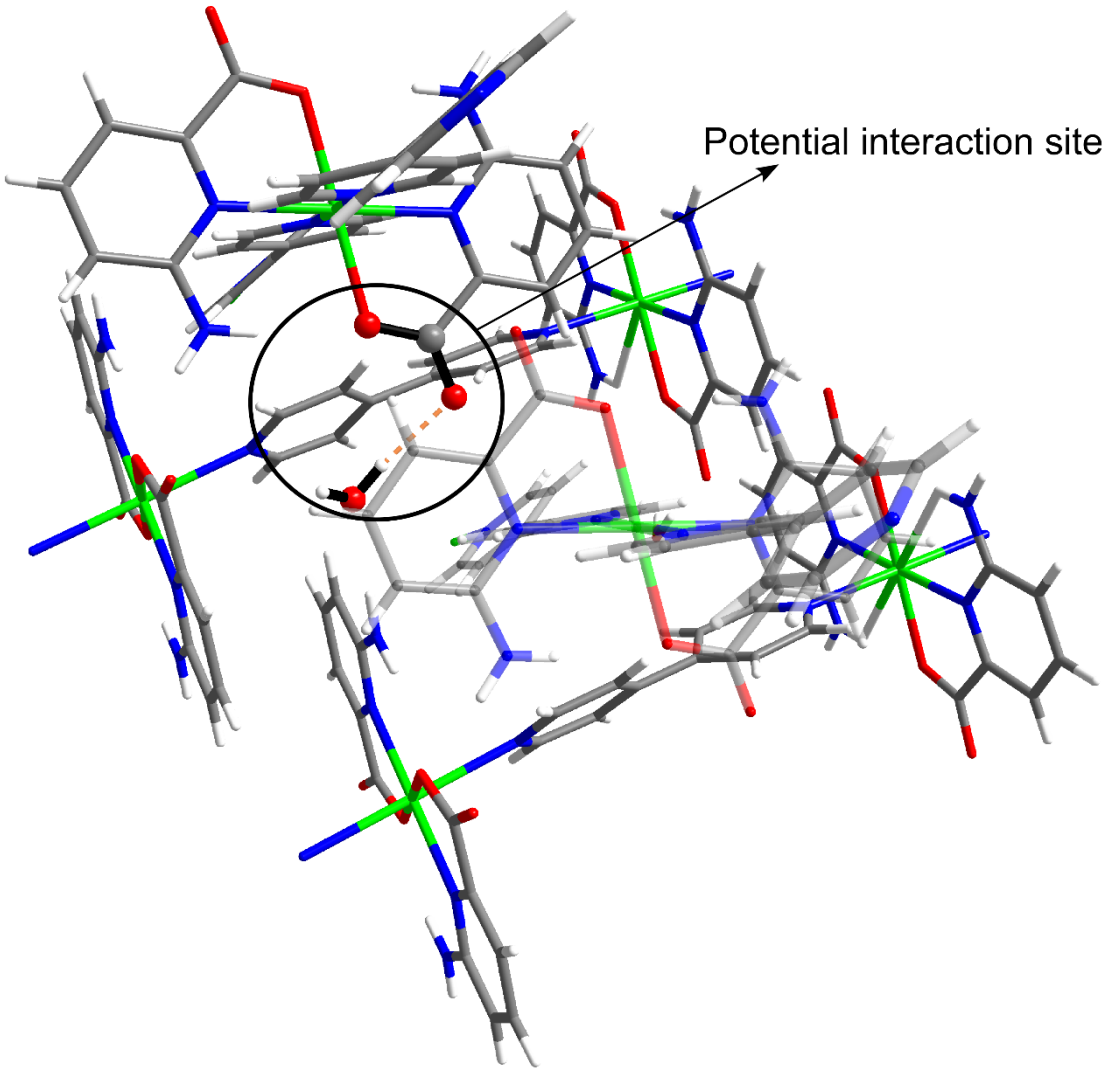


**Figure S39.** Fragment of the 3D packing of **2** showing the potential interaction site with metal ions based on a non-bonding carboxylate oxygen atom.

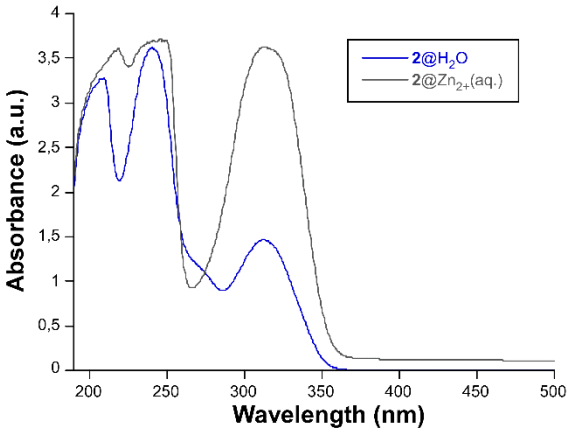


**Figure S40.** UV-Vis absorption spectra of compound **2** dispersed in water (blue line) and $Zn^{2+}$(aq) (grey line) solutions.

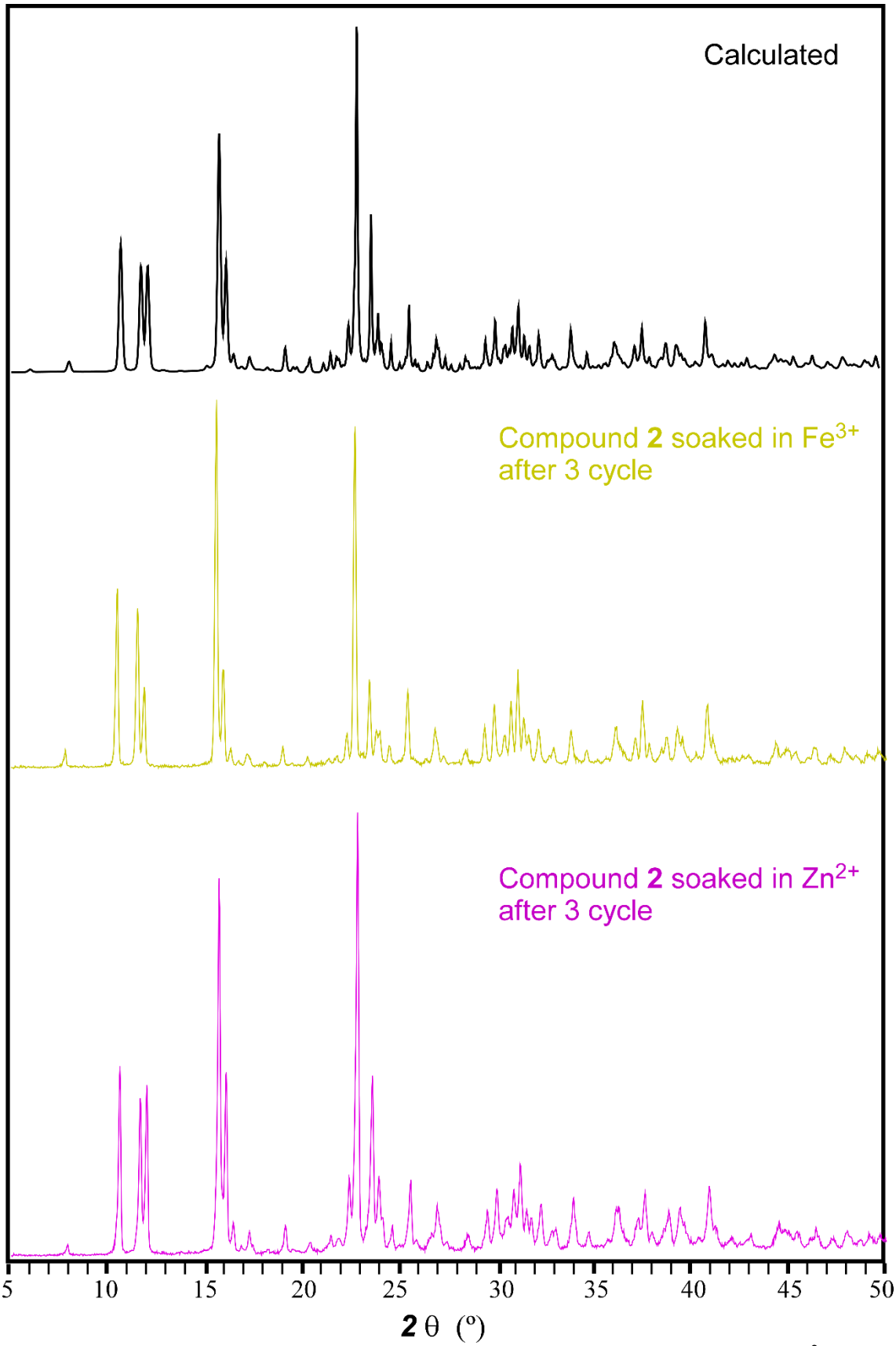


**Figure S41.** Diffraction patterns of compound **2** after the third soaking cycle into $Fe^{3+}$(aq) (yellow) and $Zn^{2+}$(aq) (purple) solutions.

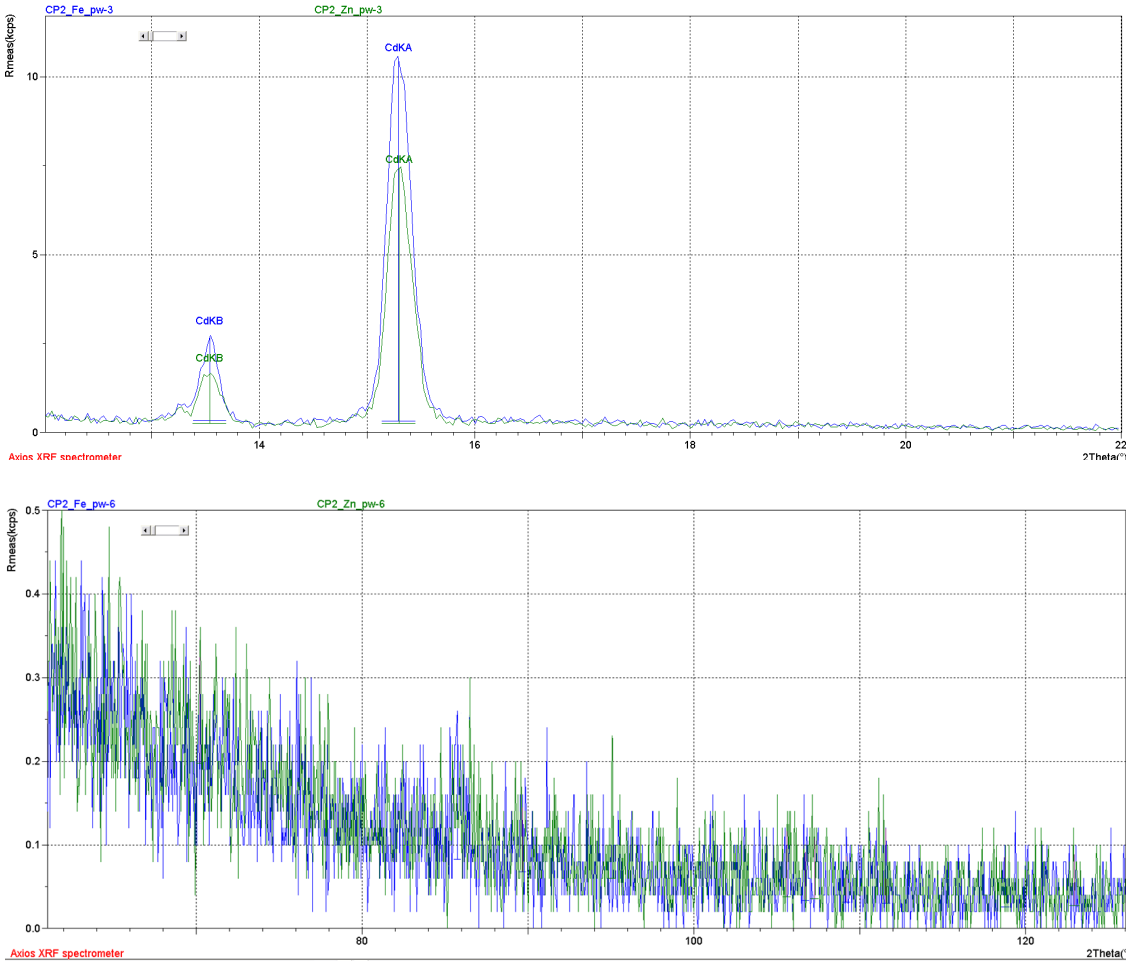


**Figure S42.** Captures of the X-ray fluorescence analysis performed over dried samples of compound **2** after the third soaking cycle into $Fe^{3+}$(aq) (blue) and $Zn^{2+}$(aq) (green) solutions, showing: **(a)** main characteristic lines of Cd and **(b)** 2θ region where the main characteristic lines for first-row transition metal ions should be displayed.

**Table S28.** A comparison of the Stern-Volmer constant ($K_{SV}$) and limit of detection (LOD) for $Fe^{3+}$ by reported sensors.

| Compound | $K_{SV}$ ($M^{-1}$) | LOD (μM) | Medium | Ref. |
|---|---|---|---|---|
| $\{[Cu_2(ttpa)_2][Cu(BPTC)]\cdot 3H_2O\cdot DMF\}_n$ | 3.82 x $10^3$ | 2.59 | $H_2O$ | [1] |
| $[ZnL(Bipy)]\cdot 0.5H_2O$ | 7.83 x $10^3$ | - | $H_2O$ | [2] |
| $[Zn_2(tpeb)(bpdc)_2]_n$ | 1.33 x $10^4$ | 0.88 | $H_2O$ | [3] |
| $\{[Zn(tba)_2]\cdot DMA\}_n$ | 4.85 x $10^4$ | - | DMF | [4] |
| $\{[Zn_3(mtrb)_3(btc)_2]\cdot 3H_2O\}_n$ | 6.50 x $10^3$ | 1.78 | $H_2O$ | [5] |
| $\{[Cd_3(itp)_2(btc)_2]\cdot 4H_2O\}_n$ | 5.88 x $10^4$ | 0.12 | EtOH | [6] |
| $\{[Cd(Hbptc)]\cdot H_2O\}_n$ | 2.56 x $10^3$ | 35 | DMF | [7] |
| $\{[Cd(bmima)_{0.5}(atp)(H_2O)]\cdot DMF\cdot 0.5H_2O\}_n$ | 3.16 x $10^4$ | 1.92 | $H_2O$ | [8] |
| $\{[Eu_2(L)_2(H_2O)_2]\cdot 5H_2O\cdot 6DMAC\}_n$ | 5.94 x $10^3$ | 0.01 | $H_2O$ | [9] |
| $\{[Eu(BCB)(DMF)]\cdot(DMF)_{1.5}(H_2O)_2\}_n$ | 2.35 x $10^4$ | 1.78 | $H_2O$ | [10] |
| $Eu^{3+}$@MIL-53-COOH(Al) | 5.12 x $10^3$ | 0.5 | $H_2O$ | [11] |
| $\{Eu(L)(BPDC)_{0.5}(NO_3)]\cdot H_3O\}_n$ | 5.16 x $10^4$ | - | DMF | [12] |
| $\{Tb(L)(BPDC)_{0.5}(NO_3)]\cdot H_3O\}_n$ | 4.30 x $10^4$ | - | DMF | [12] |
| $\{[Tb(tcmb)(H_2O)_2]\cdot 2H_2O\}_n$ | 1.49 x $10^4$ | 0.67 | $H_2O$ | [13] |
| Compound **2** | 1.56 x $10^4$ | 7.20 | $H_2O$ | This work |
| Compound **2@paper** | 7.53 x $10^5$ | 0.24 | $H_2O$ | This work |

**Table S29.** A comparison of the Stern-Volmer constant ($K_{SV}$) and limit of detection (LOD) for $Zn^{2+}$ by reported sensors.

| Compound | $K_{SV}$ ($M^{-1}$) | LOD (μM) | Medium | Ref. |
|---|---|---|---|---|
| $\{[Cd(btic)(phen)]0.5H_2O\}_n$ | 1.81 x $10^4$ | 417 | $H_2O$ | [14] |
| $\{[Cd_3(btdc)_3(DMF)_2(EtOH)_2]\cdot 2EtOH\cdot 2H_2O\}_n$ | - | - | MeOH | [15] |
| D-P6 | - | 0.03 | $H_2O$ | [16] |
| 2-(4,5-diphenyl-1H-imidazol-2-yl)-4-phenylquinoline (DIPQ) | - | 0.027 | $H_2O$ | [17] |
| 2,4-dibromo-6-((quinolin-8-ylimino)methyl)phenol | - | 0.14 | $H_2O$ | [18] |
| Carbon dots | - | 0.05 | $H_2O$ | [19] |
| Compound **2** | 1.6 x $10^3$ | 350 | $H_2O$ | This work |

## S10. TD-DFT and DFT calculations on the interaction of $Zn^{2+}$ with compound 2

The structure of the $[Cd(6apic)_2(bipy)_2]$ complex with a coordinated $Zn^{2+}$ cation was first optimized and a TD-DFT calculation was performed on that optimized fragment (Figure S49) to compare with the result of the initial calculation.

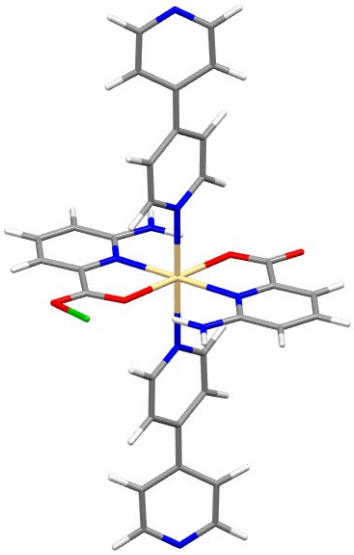

**Figure S43.** Model of optimized compound **2** with a coordinated zinc cation (**2+Zn**).

As observed in the following results, the presence of the coordinated zinc ion does not strongly shift the absorption bands of the compound but it significantly increase the oscillator strengths.

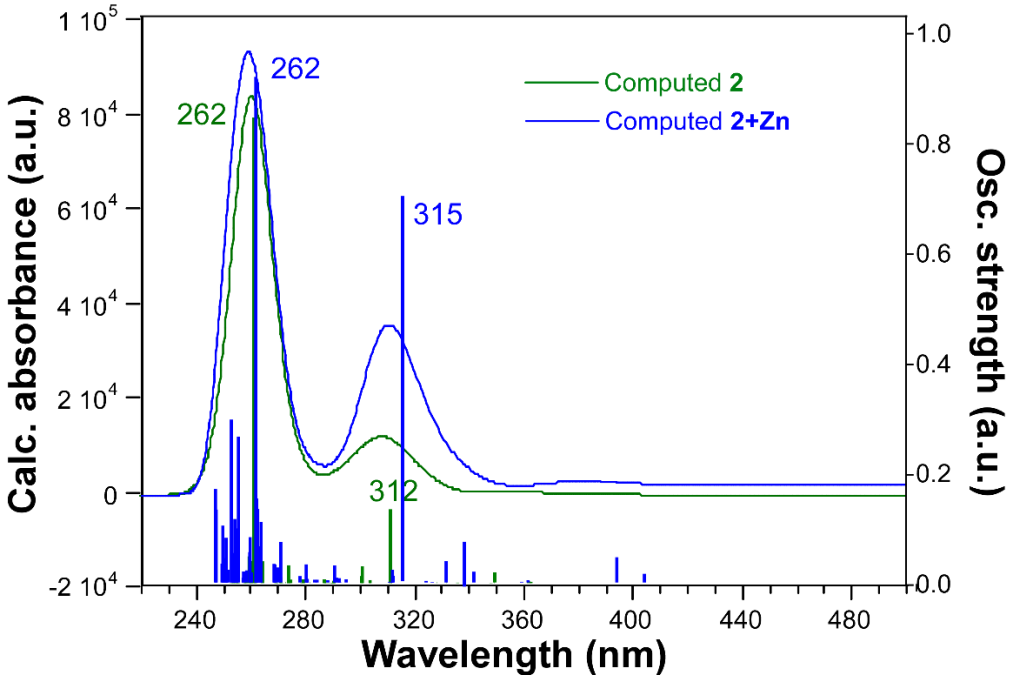


**Figure S44.** Comparison of the TD-DFT computed absorption spectra for the optimized $[Cd(6apic)_2(bipy)_2]$ model of compound **2** in the absence or presence of zinc(II) ion.

In view of the turning-on luminescence response of compound **2** in the presence of $Zn^{2+}$ ion in aqueous solution, the interaction between the ion and a representative fragment of the complex was computed. For the calculation of the energy, we assumed that $Zn^{2+}$ ion exists in the form of hexaaquocation, and that a partial replacement of a coordinated water molecule by the non-chelating carboxylate oxygen atom of a 6apic ligand will take place during the reaction summarized in the following scheme:

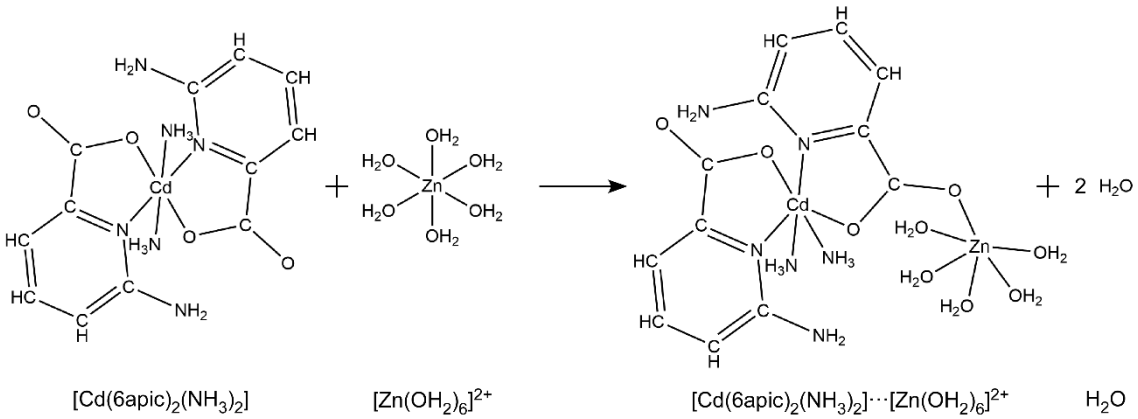


**Figure S45.** Schematic view of the computed reaction performed to estimate the interaction energy between compound **2** and the aqueous zinc cation.

The calculations were performed at DFT level of theory, with the B3LYP functional and the def2-QZPV basis set for all non-metal atoms The main results of this reaction are given in the following table:

**Table S30.** Main computed thermodynamic results of the ligand substitution reaction.

| Compound | *S* (cal $mol^{-1}$ $K^{-1}$) | Δ*H* (KJ $mol^{-1}$) | Δ*S* (KJ $mol^{-1}$) | Δ*G* (KJ $mol^{-1}$) |
|---|---|---|---|---|
| Reaction global parameters | – | -0.11 | 0.16 | -47.01 |
| $[Cd(6apic)_2(NH_3)_2]$ | 174.537 | – | – | – |
| $[Zn(OH_2)_6]^{2+}$ | 136.943 | – | – | – |
| $[Cd(6apic)_2(NH_3)_2]\cdots [Zn(OH_2)_6]^{2+}$ | 250.983 | – | – | – |
| $H_2O$ | 45.141 | – | – | – |

In view of these results, it may be concluded that the reaction is entropy-driven, probably as a consequence of the variable solvation ability of the species in the aqueous medium.

## S11. Sensing in PADs

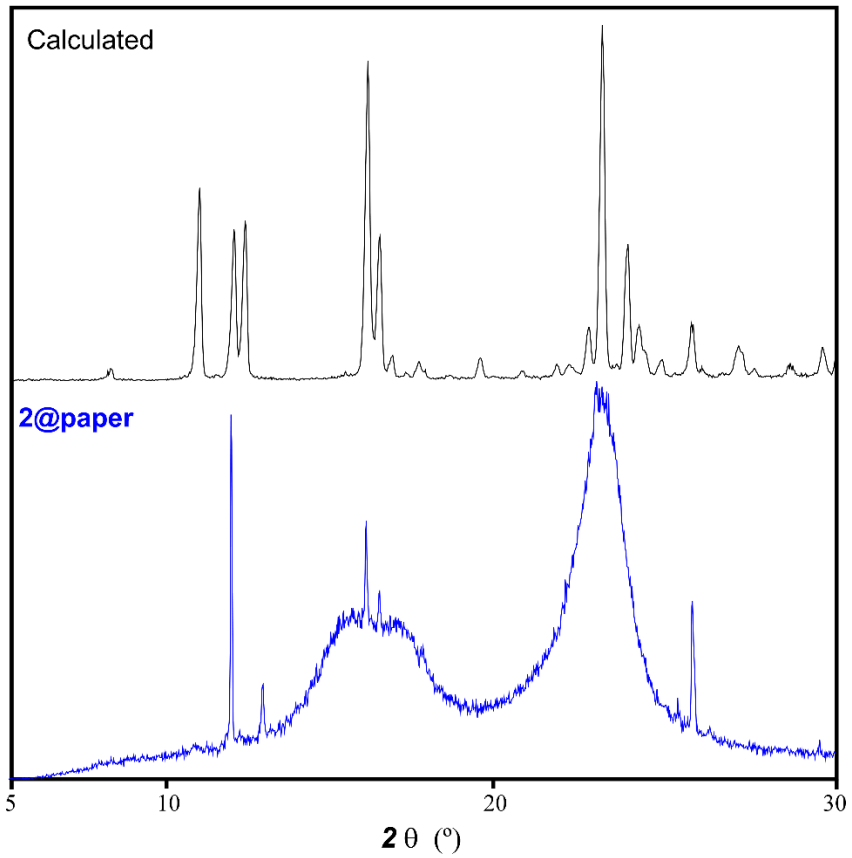


**Figure S46.** PXRD of compound **2** deposited in paper. The observed broad humps comes from the amorphous nature of cellulose.

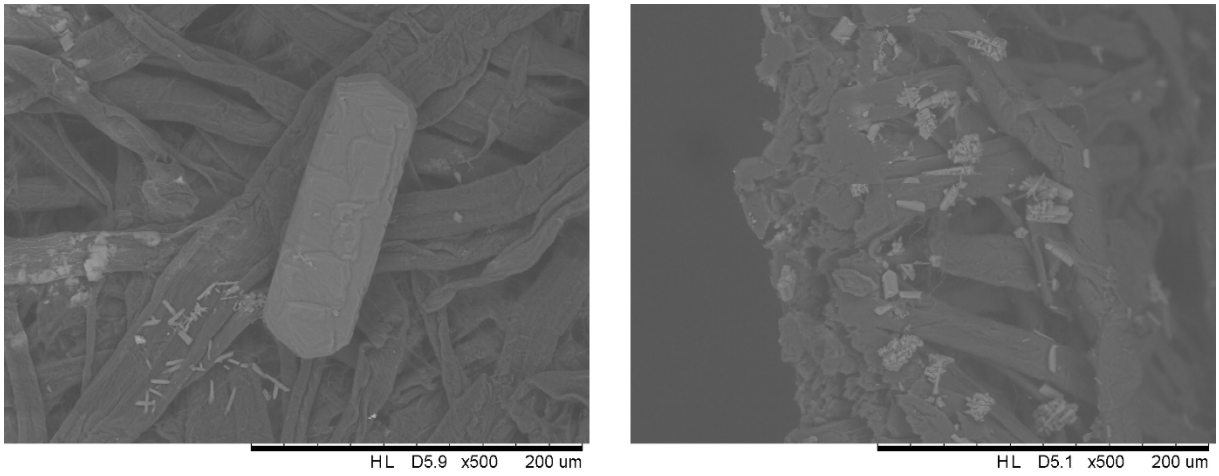


**Figure S47.** SEM images of compound **2** supported on cellulose showing frontal images (a) and a transversal image (b).

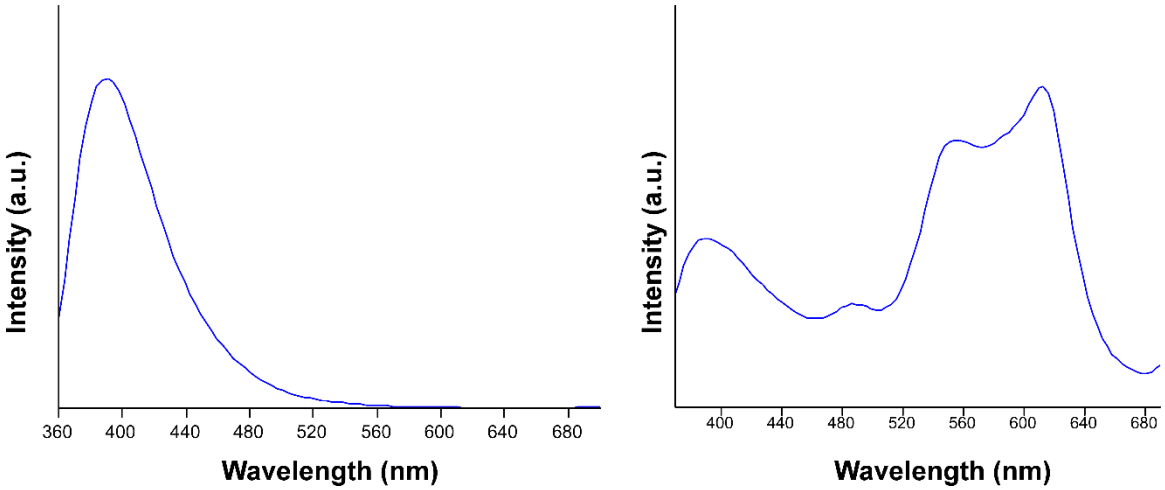


**Figure S48.** Fluorescence (left) and phosphorescence (right) emission spectra of **2@paper** at room temperature excited at 340 nm.

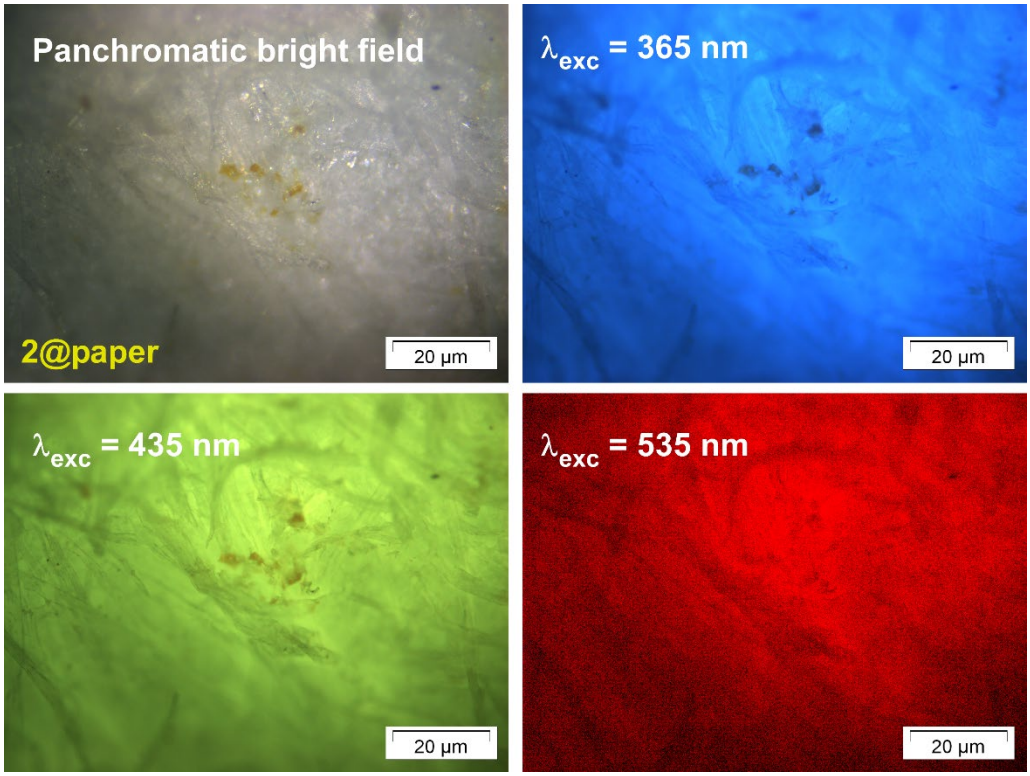


**Figure S49.** Micro-PL images taken on compound **2@paper** excited at different wavelengths at room temperature.

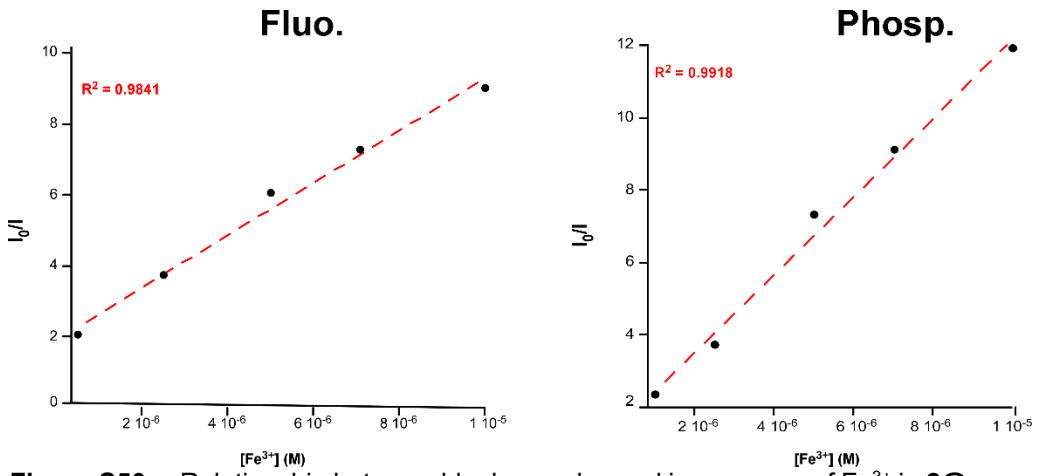


**Figure S50.** Relationship between blank samples and in presence of $Fe^{3+}$ in **2@paper** at different concentration showing the best fitting according to the Stern-Volmer plot for fluorescence (left) and phosphorescence (right).

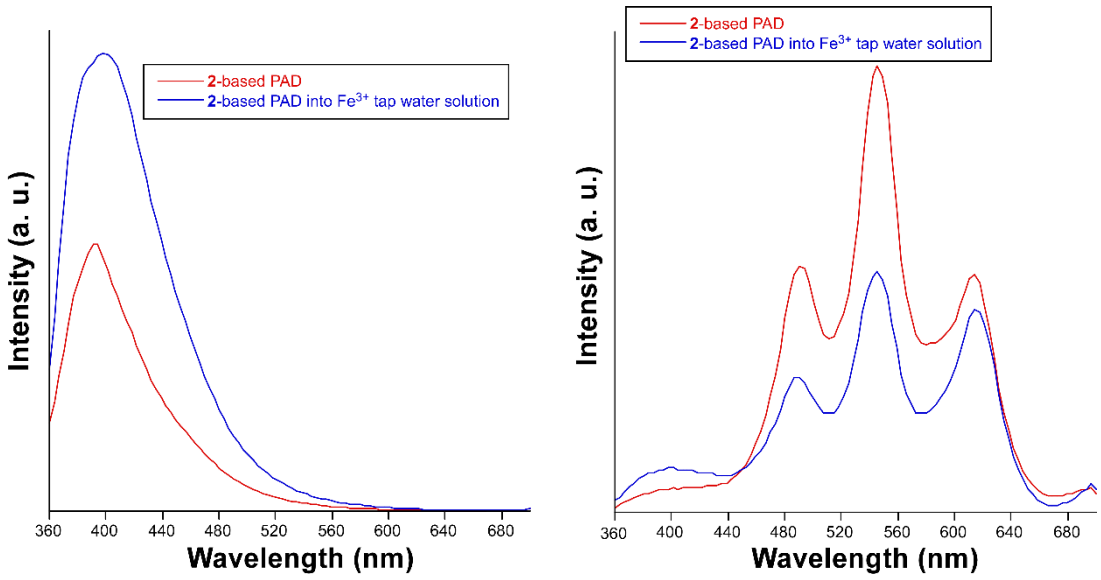


**Figure S51.** Evolution of the **(a)** fluorescent and **(b)** phosphorescent bands for the PAD before and after being immersed in solutions of tap water with 2.5 $10^{-5}$ M of $Fe^{3+}$ ion.

## S12. References


1 L.-L. Qian, Z.-X. Wang, J.-G. Ding, H.-X. Tian, K. Li, B.-L. Li and H.-Y. Li, *Dye. Pigment.*, 2020, **175**, 108159.

2 D. Wang, D. Zhang, S. De Han, J. Pan, Z. Z. Xue, J. H. Li and G. M. Wang, *Dalton Trans.*, 2019, **48**, 602–608.

3 B. B. Rath and J. J. Vittal, *Inorg. Chem.*, 2020, **59**, 8818–8826.

4 X.-D. Fang, J. Yao, R. Fan, X.-F. Bai, Y.-E. Liu, C.-F. Hou, Q.-Q. Xu, A.-X. Zhu and B. Huang, *J. Solid State Chem.*, 2021, **294**, 121854.

5 Y.-Q. Zhang, V. A. Blatov, T.-R. Zheng, C.-H. Yang, L.-L. Qian, K. Li, B.-L. Li and B. Wu, *Dalton Trans.*, 2018, **47**, 6189–6198.

6 T. R. Zheng, V. A. Blatov, Y. Q. Zhang, C. H. Yang, L. L. Qian, K. Li, B. L. Li and B. Wu, *J. Lumin.*, 2018, **199**, 126–132.

7 Y. Wang, G.-P. Yang, P.-F. Zhang, L.-L. Ma, J.-M. Wang, G.-P. Li and Y.-Y. Wang, *Cryst. Growth Des.*, 2021, **21**, 2734–2743.

8 C. Li, X. Sun, X. Meng, D. Wang and C. Zheng, *CrystEngComm*, 2023, **25**, 2728–2738.

9 J. J. Ma and W. S. Liu, *Dalton Trans.*, 2019, **48**, 12287–12295.

10 M.-Y. Zhang, F.-Y. Yi, L.-J. Liu, G.-P. Yan, H. Liu and J.-F. Guo, *Dalton Trans.*, 2021, **50**, 15593–15601.

11 Y. Zhou, H.-H. Chen and B. Yan, *J. Mater. Chem. A*, 2014, **2**, 13691–13697.

12 W. Yan, C. Zhang, S. Chen, L. Han and H. Zheng, *ACS Appl. Mater. Interfaces*, 2017, **9**, 1629–1634.

13 G. Tan, R.-Q. Jia, W.-L. Wu, B. Li and L.-Y. Wang, *Cryst. Growth Des.*, 2022, **22**, 323–333.

14 L. Liu, Y. Ran, J. Du, Z. Wang, M. Liu and Y. Mu, *RSC Adv.*, 2021, **11**, 11266–11272.

15 N. Wei, R.-X. Zuo, S. Zhang and Z. Han, *Inorganica Chim. Acta*, 2016, **453**, 305–309.

16 S. Yu, Y. Li, L. Gao, P. Zhao, L. Wang, L. Li and Y.-W. Lin, *Spectrochim. Acta Part A Mol. Biomol. Spectrosc.*, 2021, **261**, 120042.

17 K. Gavash Harsha, C. Madhu, N. Puvvada, T. Ramachandra Rao Baggi, V. Jayathirtha Rao and N. Reddy Chereddy, *ChemistrySelect*, 2020, **5**, 6059–6065.

18 P. Ghorai, K. Pal, P. Karmakar and A. Saha, *Dalton Trans.*, 2020, **49**, 4758–4773.

19 G. Lu, Z. Jia, M. Yu, M. Zhang and C. Xu, *Molecules*, 2023, 28.